Thanks a million for your precious time. According to the two referees' comments, we have modified the manuscripts point-by-point, including the followed main aspects:

1) According to Referee 1's comment, we added the model evaluation of SO_2 and NO_2. Daily observed and simulated SO_2 and NO_2 concentrations were averaged from 13 National Standard Air Quality Stations during December 2016 in Xi'an. Due to the lack of data on the implementation of desulfurization projects for important emission sources such as coal-fired power plants in recent years, the model has an obvious overestimation of SO_2. The model performance of NO_2 concentration is better. And there is high consistency of variation trend between the simulated and observed concentrations of SO_2 and NO_2, with R being 0.81 and 0.75, respectively.
2) We have revised the clearer figure caption for Figure 7.
3) We have increased the PPI of Figure11 and 12.
4) According to Referee 2's comment, we referenced the study of Yang et al. (2020) on wind speed at a 10 m altitude (W10).
5) We deleted the comparison of model performance between some urban stations and suburban stations in the manuscript, and wrote the complete evaluation results of all stations in the supplement.
6) We have used "simulation" instead of "mechanism" in the revised version.
7) Since the reviewer mentioned the language issue, the professional language copy-editing for GMD will be called for the final revised manuscript to solve the language issue. We hope this measure could further improve the presentation quality of the manuscript.

Response to Referee Comment #1:

1. The initial conditions is very important to model simulation. This manuscript investigated the duration of initial concentrations. The degree of agreement between initial conditions and observations largely the model performance in the first hours. I suggested that the authors compared initial conditions with observations. If possible, the manuscript can design different initial conditions.

Response: In our manuscripts, we have compared the simulated and observed $PM_{2.5}$ concentrations in December 2016. So here we compared the simulated and observed $PM_{2.5}$ concentrations in the sensitivity experiments of R1120, R1124, C24 and CT24 from the time of the simulation started to 00:00 UTC on December 1st, shown in Figure 1. Although the degree of agreement between initial conditions and observations had a large difference in the first hours, the results of sensitivity experiments for restart simulation showed that 27 hours of simulation can eliminate the influence of the initial value and improve the simulation results under the same emission and meteorological field. One of the best ways to improve model performance is to consider the assimilation of the initial conditions. But this technology is more difficult, we are still developing.

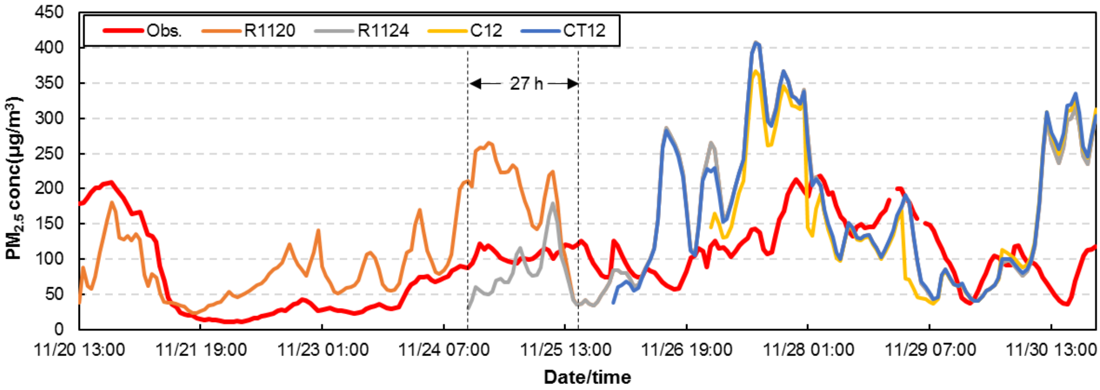

Figure 1. The time series of daily observed and simulated $PM_{2.5}$ concentrations averaged from 13 NSAQ Observation Stations from the time of the simulation started to 00:00 UTC on December 1st.

2. The impact of initial conditions is different on different species. I suggested that different components (SO_4, NO_3, NH_4, primary PM) or SO_2 NO_x were discussed.

Response: While verifying the model performance of $PM_{2.5}$ concentrations, this study also verified the model performance of sulfur dioxide (SO_2) and nitrogen dioxide (NO_2) concentrations, which are the important precursors of SO_4 and NO_3, parts of particulate matter, based on CAMx simulation under the initial restart mechanism. Figure 2 shows the time series of daily average SO_2 and NO_2 concentrations and the statistical results are listed in Table 1. The model has an obvious overestimation of SO_2, with an average bias of 156.31 μg/m^3, and the observed SO_2 concentration is only 18% of the simulated value. The main reason is that the implementation of desulfurization projects for important emission sources such as coal-fired power plants in recent years has not been fully considered, which has led to overestimation of SO_2 emissions in the emission inventory. Li et al. (2017) found that the SO_2 emissions in China have decreased by 75% during the year 2007 to 2016, that is, SO_2 emissions in 2016 were about 25% of 2007. If the simulated SO_2 concentrations are divided by 4, the statistical parameters will be greatly improved, shown in Table 1. Also the intensity of emissions reduction has uneven spatial distribution. In summary, the overestimation of SO_2 is due to the lack of relevant data. The model performance of NO_2 concentration is better, the IOA reaches 0.82, and the MB is only 3.32μg/m^3. There is high consistency of variation trend between the simulated and observed concentrations of SO_2 and NO_2, with R being 0.81 and 0.75, respectively. The variation of SO_2 and NO_2 will be added in our revised manuscripts followed this comment.

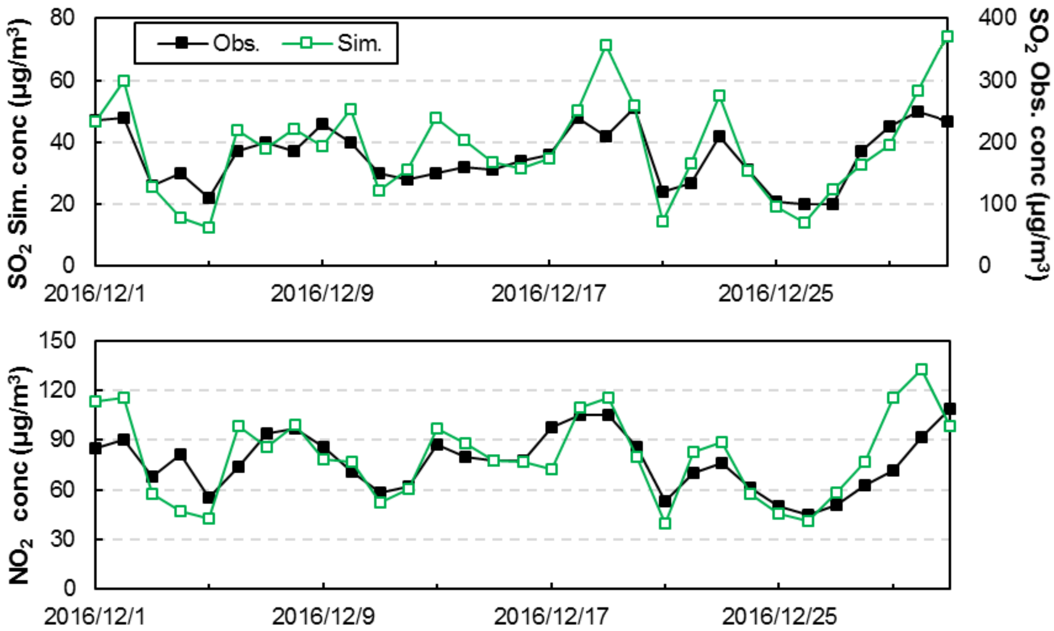

Figure 2. The time series of daily observed and simulated SO_2 (top)and NO_2 (bottom) concentrations averaged from 13 NSAQ Observation Stations during December 2016 in Xi'an. The black and green lines indicate observed and simulated results, respectively.

Table 1. Statistical verification parameters of SO_2 and NO_2 during December 2016in Xi'an.

Species	Mean(μg/m^3)		R	MB	ME	NMB	NME	RMSE	IOA
	Obs.	Sim.		(μg/m^3)	(μg/m^3)				
SO_2	35.45	191.76	0.81	156.31	156.31	4.41	4.41	171.73	0.11
SO_2/4		47.94	0.81	12.49	14.09	0.35	0.40	18.19	0.66
NO_2	76.77	80.09	0.75	3.32	12.86	0.04	0.17	17.13	0.82

And the corresponding modified contents were added to page 21, line 348 in the revised manuscript, and the reference was added to 26, line 508 as following:

4.3 Model performance of SO_2 and NO_2

The sulfur dioxide (SO_2) and nitrogen dioxide (NO_2) concentrations are the important precursors of SO_4 and NO_3, parts of particulate matter. Daily observed and simulated SO_2 and NO_2 concentrations averaged from 13 NSAQ Stations under the initial restart simulation. Figure 14 shows the time series of daily average SO_2 and NO_2 concentrations averaged from 13 NSAQ Stations under the initial restart simulation, and the statistical results are listed in Table 5. The model has an obvious overestimation of SO_2, with an average bias of 156.31 μg/m^3, and the observed SO_2 concentration is only 18% of the simulated value. The main reason is that the implementation of desulfurization projects for important emission sources such as coal-fired power plants in recent years has not been fully considered, which has led to overestimation of SO_2 emissions in the emission inventory. Li et al. (2017) found that the SO_2 emissions in China have decreased by 75% during the year 2007 to 2016, that is, SO_2 emissions in 2016 were about 25% of 2007. Also the intensity of emissions reduction has uneven spatial distribution. The model performance of NO_2 concentration is better, the IOA reaches 0.82, and the MB is only 3.32μg/m^3.

There is high consistency of variation trend between the simulated and observed concentrations of SO_2 and NO_2, with R being 0.81 and 0.75, respectively.

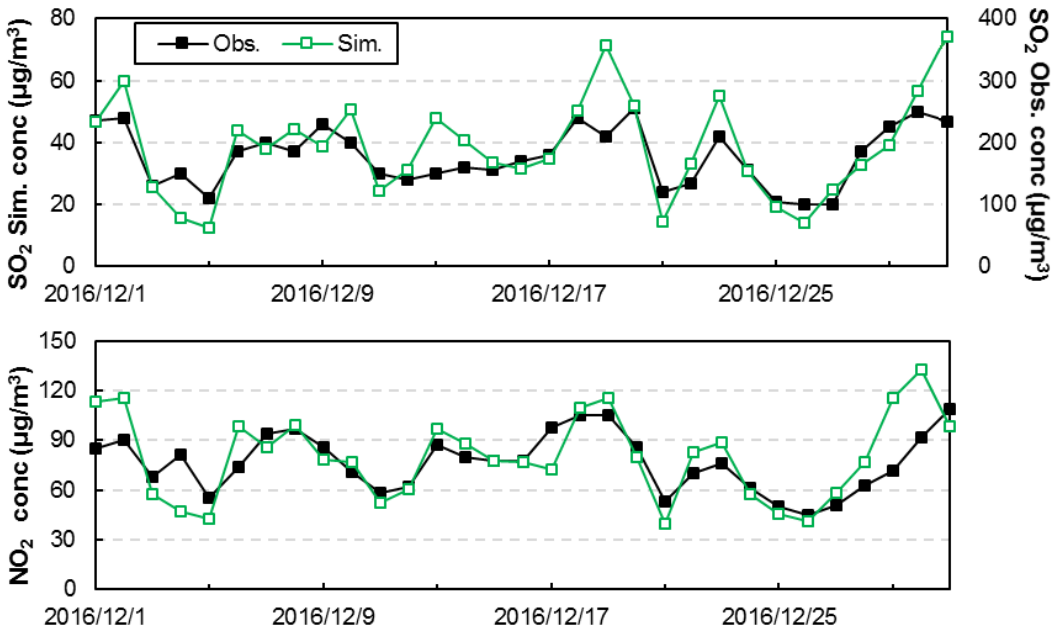

Figure 14. The time series of daily observed and simulated SO_2 (top)and NO_2 (bottom) concentrations averaged from 13 NSAQ Stations during December 2016 in Xi'an. The black and green lines indicate observed and simulated results, respectively.

Table 5. Statistical verification parameters of SO_2 and NO_2 during December 2016in Xi'an.

Species	Mean(μg/m³)		R	MB	ME	NMB	NME	RMSE	IOA
	Obs.	Sim.		(μg/m³)	(μg/m³)				
SO_2	35.45	191.76	0.81	156.31	156.31	4.41	4.41	171.73	0.11
NO_2	76.77	80.09	0.75	3.32	12.86	0.04	0.17	17.13	0.82

Li C, Mclinden C, Fioletov V, et al.: India Is Overtaking China as the World's Largest Emitter of Anthropogenic Sulfur Dioxide, Scientific Reports, 2017, 7(1):14304, https://doi.org/10.1038/s41598-017-14639-8.

3. More clear figure captions like figure 7 is needed.

Response: We have revised the figure caption. And the corresponding modified contents were added to page 12, line 230 in the revised manuscript as following:

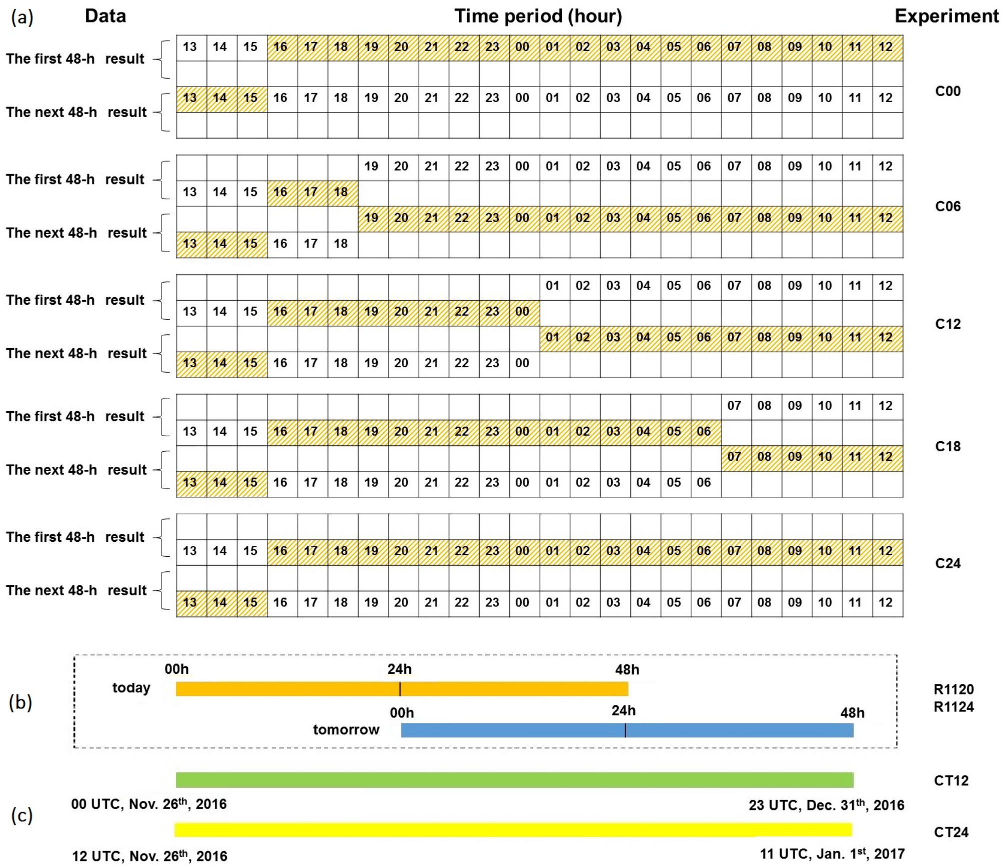

Figure 7. The time period for each initial condition experiments. **(a)** shows the time period for Clean initial condition (mark C) experiments. The first hour results in the output files of CAMx were at 13:00 UTC every day and the CAMx model forecasted the next 48 hours' $PM_{2.5}$ concentrations in each cycle simulation. The sensitivity experiments C00, C06, C12, C18, and C24 extract different time periods (0~24h, 6~30h, 12~36h, 18~42h and 24~48h, respectively) in each output file as valid data, represented by the grids with number. Each grid represents an hour and the numbers on the grids indicate the hours of the data. The grids with numbers represents the valid time period for each output file. In order to analyze from 0:00 Beijing time (16:00 UTC) every day, the 24-hour data of a day is cut and merged from 16:00 UTC in the valid time period of each output file. And the shaded grids represent the data for one single day. **(b)** shows the time period for Restart (mark R) experiments. The meteorological data of the period 12~36 h was cut to estimate the $PM_{2.5}$ concentrations by restart mechanism. The first day of the simulation starts at 12:00 UTC, and the following days starts at 00:00 UTC. **(c)** show the time period for continuous simulation (mark CT) experiments. The meteorological data of the period 12~36 h is cut and merged to one file for CT12 and the period 24~48 h was cut and merged for CT24.

4. Some figures need high PPI like Figure11 and 12.

Response: We have increased the PPI of Figure 11 and 12. The new figure 11 was added to page 17, line 311, and the new figure 12 was add to page 19, line 335 in the revised manuscript as following:

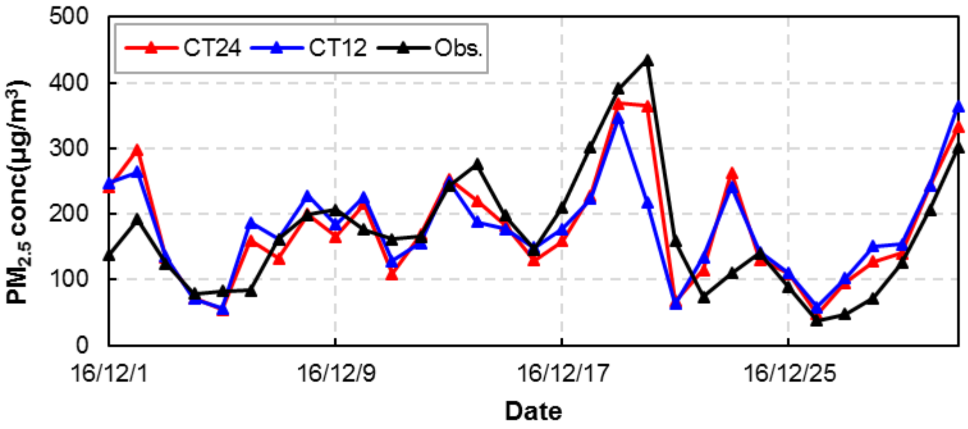

Figure 11. The time series of daily $PM_{2.5}$ concentrations for continuous simulation in Xi'an. The black line represents observations, the blue and red lines show simulated data started at November 26th 00:00UTC and November 26th 12:00UTC, respectively.

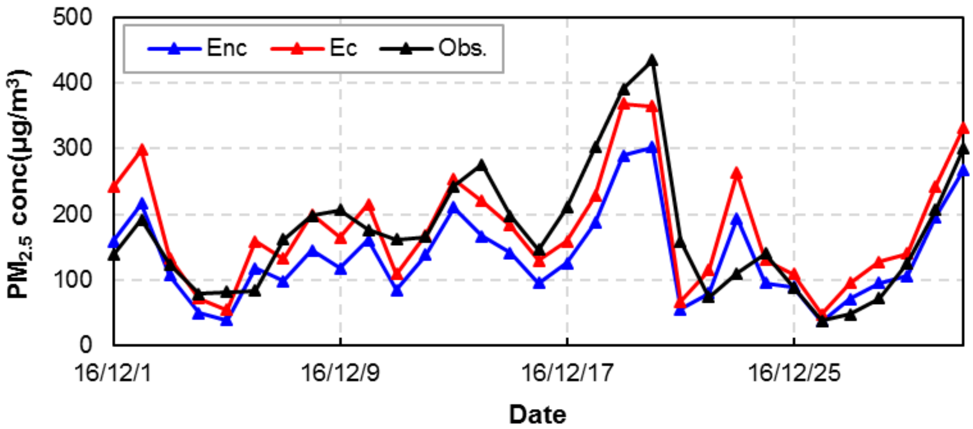

Figure 12. The time series of daily observed and simulated $PM_{2.5}$ concentrations averaged from 13 NSAQ Observation Stations during December 2016 in Xi'an. The black line represents the observations, the blue line represents the simulated by the CAMx model with construction fugitive dust, and the red line represents the simulated values without construction fugitive dust.

5. IN figures 12, Why did that simulated PM2.5 with fugitive dust emissions.is higher than that without fugitive dust emissions.

Response: Thank you for your comment. The concentrations of $PM_{2.5}$ in the model is the sum of multiple types of particulate matter, including 4 primary particulate matter (PEC, POA, FPRM and FCRS). The construction fugitive dust emissions contain primary particulate matter. So the concentrations of primary particulate matter with construction fugitive dust emissions is higher than that not including building dust emissions, resulting the total concentration of $PM_{2.5}$ with fugitive dust is higher.

Response to Referee Comment #2:

1) The simulation was done in the period of November 20, 2016 to January 20, 2017 but the comparison of simulations and observations was made only in December, 2016, why?

Response: According to the study of Yang et al. (2020), December 2016 was a month with severe $PM_{2.5}$ pollution, including a severe pollution process. Therefore, this study finally selected December 2016 for simulation and analysis. Because we did not know how long the spin-up time would take before the simulation experiments, we simulated forward 10 days as the spin-up time.

2) For model evaluation of meteorological fields, the comparison of simulated and observed wind speed and direction should be added.

Response: The comparison of simulated and observed wind speed has been done in the study of Yang et al. (2020). We used the same model configuration and monitoring sites. The simulation time period in the study of Yang et al. (2020) includes the simulation time period of this study. So the model performance was similar. As shown in Fig. 1 (Yang et al., 2020), the WRF detected the variation of meteorological elements in the pollution period. And the verification statistics were shown in Table 1(Yang et al., 2020). As the results show, the W10 is underestimated. The MB of the W10 is -0.14 m/s. The R of the W10 is 0.63, which indicates a good agreement between the observations and the model results. Owing to the particular topography of Xi'an, the wind speed is low at all times. The RMSE of the simulated W10 is only 0.96.

Due to the lack of wind direction data, and the large error in model performance of wind direction shown from previous studies, this study did not evaluate the wind direction.

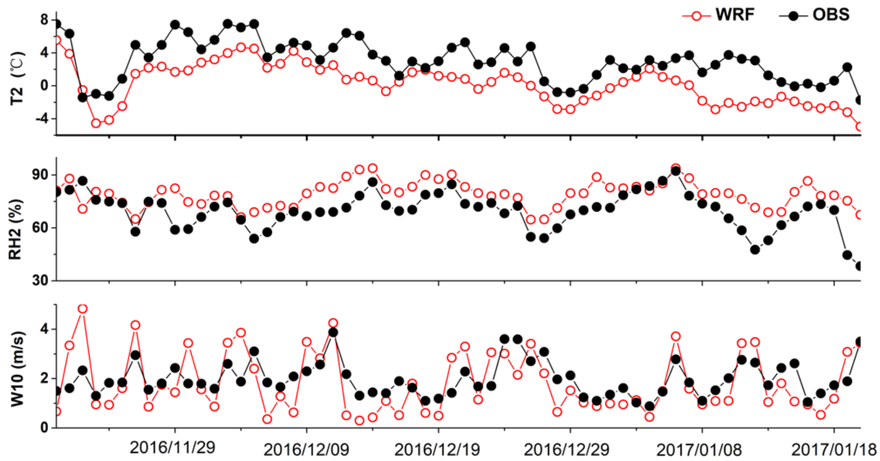

Figure 1. Time series of daily observed and simulated temperatures at a 2 m altitude (T2), relative humidity at a 2 m altitude (RH2) among nine monitoring sites, and daily average wind speed at a 10 m altitude (W10) in Xi'an station from 20 November 2016 to 20 January 2017. The black and red lines represent the observations and the values simulated by WRF. (For interpretation of the references to colour in this figure legend, the reader is referred to the web version of this article.) (Yang et al., 2020)

Table 1. Verification statistics of daily temperature at a 2 m altitude (T2), relative humidity at a 2 m altitude (RH2), and wind speed at 10 m altitude (W10) from 20 November 2016 to 20 January 2017. ME, MB, R, and RMSE are abbreviations for mean error, mean bias, correlation coefficient, root-mean-square error, and accuracy rate, respectively. The units of the Mean, ME, and MB are for T2, % for RH2, and m $s^{-1}$for W10. (Yang et al., 2020)

Variable	Mean		ME	MB	R	RMSE
	Obs.	Sim.				
T2 (℃)	3.06	0.28	2.80	-2.77	0.82	3.14
RH2 (%)	69.80	79.05	9.91	9.26	0.71	11.87
W10 (m·s-1)	1.98	1.83	0.79	-0.14	0.63	0.96

And the corresponding modified contents were added to the page 4, line 102 in the revised manuscript as following:

Under the same model configuration on WRF model and the same verified sites, Yang et al. (2020) compared the simulated and observed wind speed at a 10 m altitude (W10) in Xi'an station from 20 November 2016 to 20 January 2017. As the results show, the W10 is underestimated. The MB of the W10 is -0.14 m/s. The R of the W10 is 0.63, which indicates a good agreement between the observations and the model results.

3) The CAMx has only one domain . . .(section 2.3)? Actually, Fig.4 shows that the CAMx also has three nested domains.

Response: Fig. 4 shows the model domain in the WRF-CAMx modelling system. In this study, three-nest domains were designed for the WRF model, as shown in Figure 4. If the meteorological field only simulates one domain, directly interpolating from the initial field resolution to a 3 km-grid, the error will be relatively large. The CAMx in this study has only one domain and the settings are the same as those in the D3 domain.

4) Please explain why the model performance in the studied urban area is poorer than that in the studied counties (section 4.1.1).

Response: Thank you for your comment. We randomly selected three monitoring sites in the urban area for analysis shown in Fig 8, so the conclusion may not be rigorous enough. According to your suggestion, we checked again and verified the statistical parameters of all monitoring sites. As shown in Table 2, for correlation coefficients (R), the model performances of stations in suburban counties are better than that of some stations in urban city, indicating that the simulation of suburban counties performs better in the aspect of trends. The reason may be that PM2.5 emissions in urban areas are affected by more complex factors, and it is more difficult to simulate weather in urban areas. For bias, the model performances of stations in urban cities are better than that of the suburbs, and the simulated $PM_{2.5}$ concentrations in the suburbs are obviously underestimated. We also used the fraction of predictions within a factor of two of observations (FAC2) to verified the model performances of all the monitoring sites. The FAC2 of the urban cities is 74%, while the FAC2 of the suburban counties is 62%, indicating that the model performance of the urban area is better than that of the suburban area in terms of total emissions. We will revise the manuscript based on the following results.

Table 2. Verification statistics of PM2.5 concentrations on December 2016 among all monitoring sites.

	Station	R	MB (μg/m³)	ME (μg/m³)	NMB %	NME %	RMSE	FAC2 %
urban	CT	0.70	-58.86	66.22	-38.08	42.84	89.99	64
	XQ	0.53	61.72	81.41	36.00	47.48	108.31	75
	JKQ	0.69	-76.00	84.91	-37.55	41.95	109.89	76
	TYC	0.66	75.46	89.90	45.98	54.78	108.49	77
	GYC	0.73	19.42	52.51	11.17	30.21	68.01	89
	QJ	0.59	14.79	71.73	8.06	39.11	89.90	76
	GYT	0.62	-31.46	69.01	-18.72	41.06	84.15	66
	FZC	0.67	3.11	60.68	1.79	35.01	76.42	78
	XZ	0.57	51.62	79.66	32.64	50.36	101.86	72
	GX	0.64	67.11	88.46	39.42	51.96	104.45	69
suburban	CAQ	0.68	8.51	54.49	5.36	34.29	72.26	86
	YLQ	0.60	-97.63	99.12	-57.67	58.55	120.78	31
	LTQ	0.57	-54.43	76.28	-33.53	46.98	97.49	69

We deleted the comparison of model performance between some urban stations and suburban stations in the revised manuscript on page 14, line 270, and the corresponding modified contents were added in the **supplement** as following:

Table 1 shows the statistical results of the daily average $PM_{2.5}$ concentrations of 13 NSAQ Observation Stations during December 2016 in Xi'an. The correlation coefficients (R) of most urban stations can reach above 0.6, of which GYC is 0.73, while the R of XQ, QJ and XZ are low. Among the three stations in suburban counties, CAQ had the highest correlation coefficient of 0.68, and the other two stations are lower than 0.6. For bias, the model performances of stations in urban cities are better than that of the suburbs, and the simulated $PM_{2.5}$ concentrations in the suburbs are obviously underestimated. Except for CT, GYT and XZ, the FAC2 of the other 7 urban stations all reach more than 70%. Among the three suburban stations the CAQ has the best model performance, with FAC2 at 86%, while the other two stations are relatively low, especially the YLQ is only 31%. The average FAC2 of the urban cities is 74%, while the average FAC2 of the suburban counties is 62%, indicating that the model performance of the urban area is better than that of the suburban area in terms of total emissions.

Table 1. Verification statistics of PM2.5 concentrations on December 2016 among all monitoring sites.

	Station	R	MB	ME	NMB	NME	RMSE	FAC2

			($\mu g/m^3$)	($\mu g/m^3$)	%	%		%
urban	CT	0.70	-58.86	66.22	-38.08	42.84	89.99	64
	XQ	0.53	61.72	81.41	36.00	47.48	108.31	75
	JKQ	0.69	-76.00	84.91	-37.55	41.95	109.89	76
	TYC	0.66	75.46	89.90	45.98	54.78	108.49	77
	GYC	0.73	19.42	52.51	11.17	30.21	68.01	89
	QJ	0.59	14.79	71.73	8.06	39.11	89.90	76
	GYT	0.62	-31.46	69.01	-18.72	41.06	84.15	66
	FZC	0.67	3.11	60.68	1.79	35.01	76.42	78
	XZ	0.57	51.62	79.66	32.64	50.36	101.86	72
	GX	0.64	67.11	88.46	39.42	51.96	104.45	69
suburban	CAQ	0.68	8.51	54.49	5.36	34.29	72.26	86
	YLQ	0.60	-97.63	99.12	-57.67	58.55	120.78	31
	LTQ	0.57	-54.43	76.28	-33.53	46.98	97.49	69

5) Please use “simulation” instead of “mechanism” in the whole text.

Response: The authors thanks for your constructive suggestion. We will use “simulation” instead of “mechanism” in the revised version.

6) The writing English need more polishment.

Response: We will find the experts to help polish the writing English, and try our best to improve the level of writing English.

Numerical study of the initial condition and emission on simulating $PM_{2.5}$ concentrations in Comprehensive Air Quality Model with extensions version 6.1 (CAMx v6.1): Taking Xi'an as example

Han Xiao [1], Qizhong Wu [1*], Xiaochun Yang [1,2], Lanning Wang[1], Huaqiong Cheng[1]

[1] College of Global Change and Earth System Science, Beijing Normal University, Beijing 100875, China
[2] Xi’an Meteorological Bureau, Xi’an, Shaanxi Province 710016, China

Correspondence to: Qizhong Wu (wqizhong@bnu.edu.cn)

Abstract. A series of model sensitivity experiments is designed to explore the effects of different initial conditions and emissions in Xi’an in December 2016, which is a major city in the key area “Fen-Wei Plains” for air pollution control in China. Three methods were applied for the initial condition tests: clean initial simulation, restart simulation and continuous simulation. In clean initial simulation test, the sensitivity experiments C00, C06, C12, C18, and C24 were conducted according to the intercepted time periods, and the results showed that the model performance of $PM_{2.5}$ was better with the delay of the start time of the intercepted time periods. From experiments C00 to C24, the absolute mean bias (MB) decreased from 51.07 μg/m^3 to 3.72 μg/m^3 and the index of agreement (IOA) increased from 0.49 to 0.86, which illustrates that the model performance of C24 is much better than C00. In order to explore the restart simulation sensitivity experiments R1120 and R1124 were set according to the time of the first day for the model simulation. Although the start times of simulations were different, after a period of spin-up time, the simulation results with different start time were nearly consistent, the results showed that the spin-up time is about 27 hours. As for the continuous simulation test, CT12 and CT24 were conducted. The start time of the intercepted time periods for CT12 and R1120 were the same, and the simulation results were nearly identical. The simulation results of CT24 performed best in all the sensitivity experiments, with the correlation coefficient (R), MB, and IOA reaching 0.81, 6.29 μg/m^3, and 0.90, respectively. For the emission tests, the updated local emission inventory with construction fugitive dust emissions have been added and compared to the simulation results of the original emission inventory. The simulation with the updated local emissions showed a much better performance on $PM_{2.5}$ modelling. Therefore, combining the method of CT24 with the updated local emission inventory can nicely improve the model performance of $PM_{2.5}$ in Xi'an, the absolute MB decreased from 35.16 μg/m^3 to 6.29 μg/m^3 and the IOA reached 0.90.

删除的内容: mechanism
删除的内容: mechanism
删除的内容: mechanism
删除的内容: mechanism

1 Introduction

In the recent years, severe air pollution has gradually become a big challenge in China and other developing countries (Wu et al., 2014; Li et al., 2017a). China released three-year action plan for cleaner air in 2018, and efforts will be focused on areas including the Beijing-Tianjin-Hebei region, the Yangtze River Delta, and the Fen-Wei Plains. As a major city in the key area “Fen-Wei Plains”, Xi’an is located in the Guanzhong Basin. The city is surrounded by the Qinling Mountains to the south, and the Loess Plateau extends to the north and west, which is not conductive to the spread of air pollutant. Xi'an has suffered serious air pollution in recent years because of its special topography and rapid economic development (Zhang, et al., 2002; Cao, et al., 2012). Worse, Xi'an is under rapid development of urban construction activities with large construction fugitive dust (Long et al., 2016).

Air quality modelling systems is an important tool for air pollution assessment and have evolved over three generations since the 1970s, driven by crucial regulations, societal and economic needs, and increasing high performance computing capacity (Zhang et al., 2012). Various air quality models are widely used in the simulation and forecasting of pollutants, such as the Community Multiscale Air Quality (CMAQ) (Eder and Yu, 2006; Appel et al., 2017), the Comprehensive Air Quality Model with extensions (CAMx) (ENVIRON, 2013), WRF-Chem (Grell et al., 2005), and the Nested Air Quality Prediction Modeling System (GNAQPMS/NAQPMS) (Wang et al., 2006; Chen et al., 2015; Wang et al., 2017). In order to accurately analyze the apportionment of emission categories and contributions from different source regions for atmospheric pollutions, many researchers used the CAMx model with the particulate matter source apportionment technology (PSAT) in different areas of China, including Beijing (Zhang et al., 2018), Tangshan (Li et al., 2013), Pearl River Delta region (Wu et al., 2013) and Yangtze River Delta region (Li et al., 2011). The CAMx showed good model performances for simulation of air pollution (Panagiotopoulou et al., 2016).

The input files for CAMx model include initial/boundary conditions, gridded and elevated point source emissions, and meteorological files (ENVIRON, 2013). The meteorology and emissions inputs can cause great uncertainty for air quality models (Tang et al. 2010; Gilliam et al., 2015). Many researchers reduced the uncertainty of meteorology through refined physical parameterizations and other techniques such as data assimilation (Sistla et al., 1996; Seaman, 2000; Gilliam et al., 2015; Li et al., 2019). A reasonable emission inventory is very important for the simulation accuracy of the air quality model. Many researchers studied East Asian emissions (Kato et al., 1992; Streets et al., 2003; Ohara et al. 2007; Zhang et al., 2009;), and tried to construct emission inventories of particulate matter (PM) in China (Wang et al. 2005; Zhang et al. 2006). However, the absence of detailed information on China introduces great uncertainty into the emission inventories (Cao et al., 2011). In recent years, more and more researchers focused on constructing and updating of regional local emission inventories to improve the model performance. Wu et al. (2014) improved the model performance by adding more regional point source emissions and updating the area source emissions in village and surrounding cities of Beijing. Based on that work, Yang et al. (2019) have added local datasets into the emission inventory of Guanzhong Plain, China, which was applied in simulating $PM_{2.5}$ concentrations by CMAQ model in Xi'an. Numerous works indicated that construction dust emission plays an important role of the air pollution, especially in urban areas (Ni et al., 2012; Huang et al., 2014; Wang et al., 2015). In our previous study, we built a particulate matter emission inventory from construction activities at county level in Xi'an, based on an extensive survey of construction activities and combining with two sets of dust emission factors for the typical city in north China (Xiao et al., 2019).

However, few studies have investigated the effects of initial condition on the simulation or prediction of $PM_{2.5}$ concentrations. Therefore, the purpose of this study was to explore the effects of different initial simulation and emissions on

删除的内容: mechanism

the model performance of $PM_{2.5}$ in the CAMx model. A series of model sensitivity experiments for the initial simulation and emissions are designed to find a suitable method for simulating $PM_{2.5}$ concentrations with the reasonable initial condition and emission inventory. Not only for Xi'an, other cities may apply the similar research method using for simulating $PM_{2.5}$ concentrations in the future.

删除的内容: mechanism

The paper is organized as follows. Section 2 gives the model descriptions for WRF-SMOKE-CAMx model system, including meteorological fields, air quality model descriptions, model domain, emission inventory and processes in Sects 2.1-2.4. Section 3 presents the sensitivity experiments design of different initial condition and emission. Section 4 discuss the model performance of the initial condition tests and emission tests to simulate the $PM_{2.5}$ concentration model in Xi'an. The conclusions are given in Section 5.

2 WRF-SMOKE-CAMx model descriptions

In this study, the National Center for Atmospheric Research (NCAR) Weather Research and Forecasting (WRF v3.9.1.1) model (Skamarock et al., 2008), the Center for Environmental Modeling for Policy Development (CEMPD) Sparse Matrix Operator Kernel Emissions (SMOKE v2.4) (Houyoux and Vukovich, 1999) and the Ramboll Environ Comprehensive Air Quality Model with Extensions (CAMx v6.1) (ENVIRON, 2013) were used to build up the air quality model system as shown in Fig.1. The WRF model provided the meteorological conditions for the SMOKE and CAMx model. And the SMOKE model was used to process the emissions data and provide 4-D, model-ready gridded emissions for the air quality model CAMx.

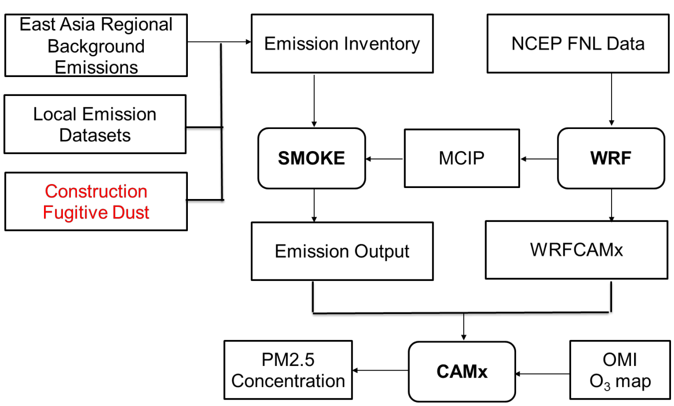

Figure 1. The framework of the WRF-SMOKE-CAMx model system in Xi’an. OMI O_3 map prepares ozone column input files for CAMx to improve the photolysis rate calculation. The CAMx forecasted the air pollutant for the next 48 hours.

2.1 Meteorological fields

For the WRF model configuration, we chose the rapid radiative transfer model (RRTM; Mlawer et al., 1997) and the Dudhia for longwave and shortwave radiation options (Dudhia, 1989), WSM3 cloud microphysics (Hong et al., 2004), the YSU scheme (Hong et al., 2006), the Kain–Fritsch (new Eta) cloud parameterization (Kain, 2004), and 5-layer thermal diffusion scheme (Dudhia, 1996). The meteorological initial and boundary conditions were derived from the National Centers for Environmental Prediction (NCEP) global final analysis data (FNL), with spatial resolution of 1° ×1° and temporal resolution of 6-h. The simulation was performed for the period of November 20, 2016 to January 20, 2017.

The simulation effect of daily average temperature (T2) and relatively humidity (RH2) simulated by WRF model in domain 3 were primarily validated by the observation data at 7 monitoring stations in Xi'an, which the station map was shown in Fig.2. Some statistical parameters of Appendix A were used to evaluate the model performance and shown in Table 1, and the time series was shown in Fig 3. The ME, R and RMSE of daily average T2 are 1.37℃, 0.80, 1.65℃, respectively, and the simulation shows cooling bias of -0.95℃. The ME and RMSE of daily average RH2 are 6.77% and 8.30%. The correlation coefficient of the relatively humidity is 0.71, which is reasonable. RH2 was slightly overestimated as the MB is 6.22%.

In previous studies, Yang et al. (2019) used WRF to drive CMAQ model for winter air quality in Xi'an, and the model evaluations for winter in 2016 showed that the MB, ME, R and RMSE of T2 were -2.83℃, 2.83℃, 0.89, 3.29℃, respectively. And the MB, ME, R and RMSE of RH2 were 9.59%, 10.63%, 0.71, 13.43%, respectively. Wu et al. (2010) used the fifth-generation NCAR/Penn State Mesoscale Model (MM5) as meteorological driver for the Nested Air Quality Prediction Modeling System (NAQPMS), and the statistical results showed that the MB and R of T2 were 2.1℃ and 0.84 and those of RH2 were -15.8% and 0.65. Under the same model configuration on WRF model and the same verified sites, Yang et al. (2020) compared the simulated and observed wind speed at a 10 m altitude (W10) in Xi'an station from 20 November 2016 to 20 January 2017. As the results show, the W10 is underestimated. The MB of the W10 is -0.14 m/s. The R of the W10 is 0.63, which indicates a good agreement between the observations and the model results.

Compared with previous studies, T2 and RH2 in this study have lower MB, ME, and RMSE. The R of T2 is slightly lower than previous studies, while the R of RH2 is higher. Thus, the meteorological simulation of this study is reasonable.

删除的内容: monitoring

删除的内容:

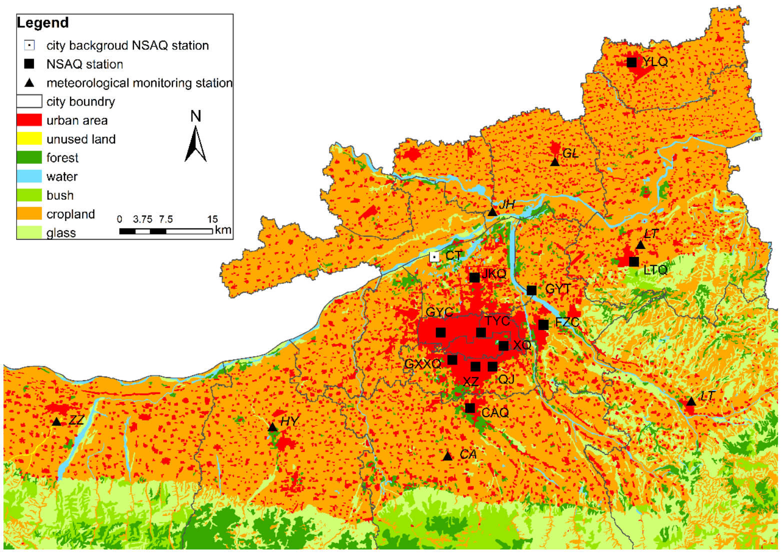

Figure 2. The stations map of the meteorological and air quality monitoring network in Xi'an. The triangles are the meteorological monitoring stations. The square with dot is the city background station and the black squares are the National Standard Air Quality Observation (NSAQ) Stations: Gaoyachang (GYC), Xingqing (XQ), Fangzhicheng (FZC), Xiaozhai (XZ), Tiyuchang (TYC), Gaoxinxiqu (GXXQ), Jingkaiqu (JKQ), Qujiang (QJ), Gaoyuntan (GYT), Changanqu (CAQ), Yanliangqu (YLQ), Lintongqu (LTQ), and Caotan (CT) Station.

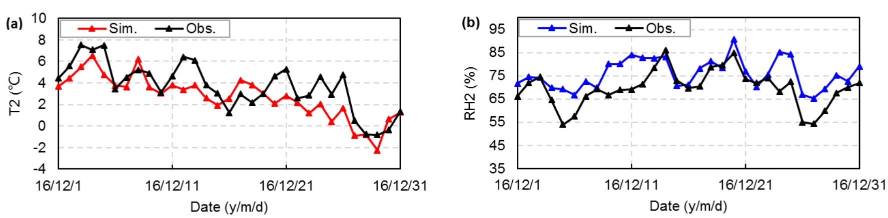

Figure 3. Time series plots of **(a)** daily average simulated and in situ 2m temperature (T2) as well as **(b)** simulated and in situ 2m relatively humidity (RH2) at the Xi'an station.

Table 1. Verification statistics of daily temperature at 2m height (T2), relatively humidity at 2m height (RH2).

Variable	Mean		ME	MB	R	RMSE
	Obs.	Sim.				
T2(℃)	3.68	2.73	1.37	- 0.95	0.80	1.65
RH2(%)	69.65	75.88	6.77	6.22	0.71	8.30

2.2 Air quality model descriptions

The CAMx model is a state-of-the-science air quality model, which is developed by the Ramboll Environ (http://www.camx.com). In this study, the PPM advection scheme (Colella and Woodward, 1984) is used for horizontal diffusion, and the K-theory is selected for vertical diffusion. The Regional Acid Deposition Model (RADM-AQ) (Chang et al., 1987) scheme as the aqueous-phase oxidation, ISORROPIA (Nenes et al., 1999) as inorganic aerosol thermodynamic equilibrium, and CB05 (Yarwood et al., 2005) as the gas-phase chemical mechanism, and the Euler-Backward Iterative (EBI) solver with Hertel's solutions (Hertel et al., 1993) is used in the model system. The resistance model for gases (Zhang et al., 2003) and aerosols (Zhang et al., 2001) in dry deposition module, and scavenging model for gases and aerosols (Seinfeld and Pandis, 1998) in wet deposition module is chosen in this study. The CAMx model forecasted the next 48 hours' $PM_{2.5}$ concentrations in clean initial simulation testing and will be described more in Sec. 2.3. On the first day, CAMx used the results of the ICBCPREP which can prepare simple, static CAMx initial condition (IC) and boundary condition (BC). On the following days, it used the different initial conditions of the sensitivity experiments.

删除的内容: mechanism

2.3 Model domain

Three-nest domains were designed for the WRF model (Fig. 4), with a horizontal resolution of 27 km × 27 km (D1), 9 km × 9 km (D2) 3 km × 3 km (D3), respectively. The biggest domain (D1) covered the most parts of China, the second domain (D2) includes Shaanxi Province, Shanxi Province, Henan Province and the inner domain (D3) focused on the 11 cities in Fen-wei Plain, including Xi'an. The CAMx has only one domain and the settings are the same as those in the D3 domain, while focusing on Xi'an as one sensitivity test area for initial conditions and emissions. To reduce the boundary effects, the CAMx model cut down the outermost grid of WRF model and used the variable of the center grid in WRFCAMx module, thus, the CAMx model was three grid cells smaller than the WRF model in D3 domain. The vertical resolution of WRF was 37 layers from the ground to 5 hPa at the top, and 14 layers were extracted by the WRFCAMx module, which can convert the WRF output files into the data format for CAMx model.

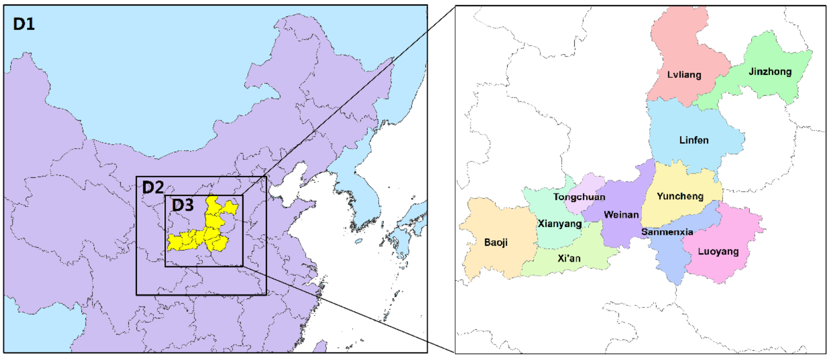

Figure 4. The three-nest model domain with 27-9-3 km horizontal resolution in the WRF-CAMx modelling system. D1 covers most parts of China, with 148 × 121 grids, and D2 includes Shaanxi, Shanxi and Henan Provinces. The inner domain covers Fen-wei Plain, including Xi'an.

2.4 Emission Inventory and Processes

The SMOKE version 2.4 (Houyoux and Vukovich, 1999) model was used to improve the Fen-wei emissions, especially Xi'an local emissions, and provide the gridded emissions for CAMx model in this study. Based on the emission inventories of previous study (Yang et al., 2019), this study added the emissions quantity of $PM_{2.5}$ from construction fugitive dust in Xi'an to update the local emission inventories. The emission inventories in this study including:

1. The regional emissions in East Asia and the local emissions in Guanzhong plain were obtained from Wu et al. (2014) and Yang et al. (2019). Major industrial emissions had a little adjusted according the annual report in this study. The emission inventory in city-level is presented in Table.2.
2. Construction fugitive dust emissions in Xi'an, based on the survey data of construction projects in Fig. 5, were collected in the previous study (Xiao et al.,2019), indicated as "local area source". This is new dataset at the county level and update in the 2017. The basic data included the location and area of each construction project. Also we replenished the missing construction data and correct the error information with Google Earth and other geographic information tools to get more accurate location information. According to statistics, there were 1595 construction projects in Xi'an in 2017, with 86.1km^2 of the total construction area. The construction area in the main urban (Xincheng, Beilin, Lianhu, Yanqiao, Weiyang and Yanta) was about 62.2km^2, accounting for 7.5% of the total area in the main urban. The distribution of the construction fugitive dust emissions in Xi'an is shown in Fig. 6.

We took the statistics-allocation approach to generate gridded area source emissions, which was to allocate the total emissions to each horizontal model grid according to the related spatial factors. In this study, the Land Scan 2015 Global Population Database (Dobson et al., 2000) was used as a spatial factor of population to allocate the emissions. For the construction fugitive dust emissions, we used the area of each construction project as the weight in the surrogate calculation, allocated the input construction projects data to the target polygons (map of administrative division in Xi'an at the county level) based on weighted spatial overlap of the input data and target polygons. And the spatial results provide to the SMOKE model as spatially allocated factor. The horizontal and vertical allocation of point source emissions were assigned from their longitude-latitude coordinates and the Briggs algorithm (Briggs, 1972; 1984), respectively. While the temporal variation and chemical species allocation were based on profile files in SMOKE model.

As shown in Table 2, the NOx emissions ranged from 352.0 kt yr^{-1} to 758.5 kt yr^{-1} between 2008 in Zhang et al. (2009) to 2017 in this study. For PM_{10} emissions in Shaanxi Province, the emissions also increased from 474.0 kt yr^{-1} to 830.0 kt yr^{-1}. PM_{10} emission in this study are higher than others, because including the construction fugitive dust. Other emission species such as NOx, SO_2, NH_3, VOCs and CO are little higher in this study than previous studies.

Table 2. Emission of major anthropogenic species in Shaanxi Province (Unit: 10^3 tons yr^{-1}).

		CO	NO_X	VOCs	NH_3	SO_2	PM_{10}	$PM_{2.5}$
This study	point source	1196.0	534.4	1572.7	-	724.7	321.7	257.5
	area source	3272.5	224.1	471.9	294.0	490.2	508.3	244.9
	Xi'an	964.1	177.5	370.5	23.4	155.4	198.6	82.8
	Baoji	628.3	65.8	256.9	32.8	131.0	68.4	41.1
	Xianyang	773.9	93.2	584.5	25.9	173.0	88.6	66.8
	Tongchuan	80.6	45.0	32.2	4.4	27.5	60.5	32.3
	Weinan	561.9	140.3	500.9	30.5	224.7	132.6	103.7
	Shaanxi Prov.	4468.5	758.5	2044.6	294.0	1214.8	830.0	502.3
Zhang et al. 2009	Shaanxi Prov.	3528.0	352.0	491.0	-	907.0	474.0	328.0
CCCPSC, 2011	Shaanxi Prov.	-	521.2	-	-	938.7	580.1	-
Yang et al. 2019	Shaanxi Prov.	4369.0	736.9	1994.1	293.2	1193.7	770.4	534.9
Yang et al. 2020	Shaanxi Prov.	3905.8	575.7	1904.3	287.6	802.3	564.0	398.1

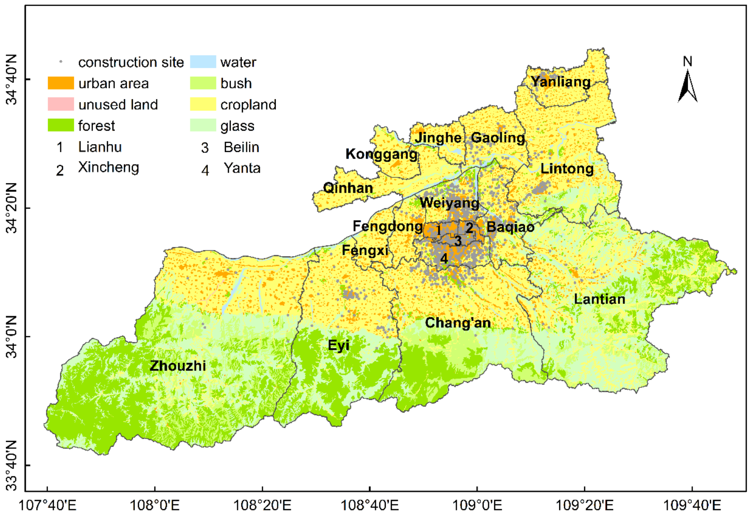

190 **Figure 5.** Spatial distribution of construction sites in Xi'an. Gray dots indicate the construction sites. The base map shows the types of land use (Xiao et al., 2019).

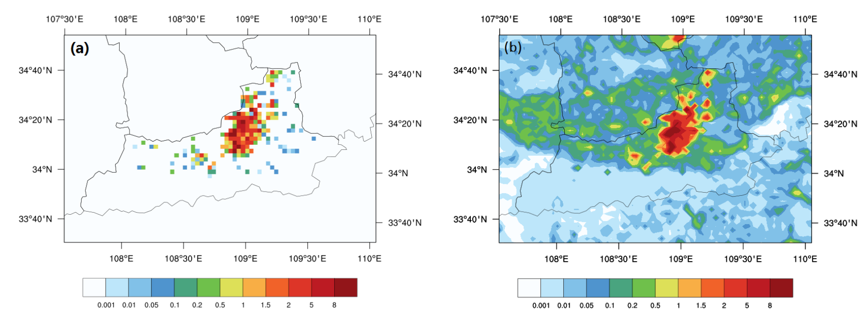

Figure 6. The spatial distribution of PM_{10} emissions in Xi'an and its surrounding area. (a) only construction fugitive dust in Xi'an. (b) all surface PM_{10} emissions in Xi'an. The grid size is 3 km x 3 km. Unit: g/km^2·s

3 Sensitivity experiments design

A set of model sensitivity experiments under different initial conditions and emissions are designed in this study. Three methods were applied for the initial condition tests: using the clean initial condition files as clean initial simulation, using the restart files as restart simulation and the continuous simulation. For the emission tests, we compared the simulation results of the original emission inventory and the updated local emission inventory with construction fugitive dust emissions. The configurations of the simulation sensitivity experiments are shown in Table 3, and the time period for each initial condition experiments are shown in Fig. 7.

删除的内容: mechanism

删除的内容: mechanism

3.1 ICON test for using the clean initial condition files

For using the clean initial condition files, icbcprep module used a clean-troposphere vertical profile to generate the initial concentration fields for each day of simulation. The output files of CAMx were initialized at 13:00 UTC. The CAMx model forecasted the next 48 hours' $PM_{2.5}$ concentrations in each cycle simulation. By extracting data from simulated results based on different time periods (0~24h, 6~30h, 12~36h, 18~42h and 24~48h, respectively) shown in Fig. 7 (a), we conducted the sensitivity experiments C00, C06, C12, C18, and C24, and explore the influence of different time periods on the simulation effect of $PM_{2.5}$. For the sensitivity experiment C00, the data of the period for the first 24 h of output file was cut and merged to analyze. And for C06, the first 6 h of data was spin-up time, we cut and merged the data of the period from 19:00 UTC to 18:00 UTC in the second day. C12, C18 and C24 were used the same method to extract and merge data, and the spin-up time of them was the first 12 h, 18 h and 24 h of data, respectively.

3.2 ICON test for using the restart files

The meteorological data of the period 12~36 h was cut to estimate the $PM_{2.5}$ concentrations by restart simulation of CAMx model. For using the restart files, icbcprep module also used clean initial concentration fields at the beginning of the first-day simulation. And gridded three-dimensional instantaneous concentrations of all species on all grids were written at the end of the simulation to allow for a model restart. Then ICON used the 24-h forecast results from the day before as the initial conditions for the following days shown in Fig. 7 (b). The first day of the simulation starts at 12:00 UTC, and the following days starts at 00:00 UTC. In order to explore how long is the spin-up time can eliminate the error caused by the initial value, the sensitivity experiments R1120 and R1124 were set according to the time of the first day for the model simulation, which began on November 20th, 2016 and November 24th, 2016, respectively.

删除的内容: mechanism

3.3 ICON test for continuous simulation

For the continuous simulation, sensitivity experiments CT12 and CT24 were set according to the start time of the intercepted time periods, which were started at 00:00UTC and 12:00UTC, respectively, shown in Fig. 7 (c). For CT12, the meteorological data of the period 12~36 h was cut and merged to one file. The period 24~48 h was cut and merged for CT24. Also we built the continuous emission files by SMOKE model. During the simulation, there was no interruption and finally generated a long-term sequence simulation result for each start time.

3.4 Emission test for different emission inventories

Based on the initial condition tests, we selected the best method to do the emission sensitivity experiments. For the emission tests, we compared the simulation results of the original emission inventory (sensitivity experiments Enc) and the updated local emission inventory with the construction fugitive dust emissions (sensitivity experiments Ec).

Table 3. The simulation experiment configurations. C00-C24, R1120, R1124, CT12 and CT24 were used to investigate the impact of simulation methods, start time and extracted time period. The impact of different emission inventory was investigated by Ec and Enc. Method C, R, CT presented for the methods of the clean initial condition simulation, restart simulation and continuous simulation. Emission inventory nc and c presented for the original emission inventory and the updated local emission inventory with the construction fugitive dust emissions, respectively.

删除的内容: mechanism

删除的内容: mechanism

Experiment	Method	Emission inventory	Start time and extracted time period
C00	C	c	2016/11/26 0-24th hour
C06	C	c	2016/11/26 6-30th hour
C12	C	c	2016/11/26 12-36th hour
C18	C	c	2016/11/26 18-42th hour
C24	C	c	2016/11/26 24-48th hour
R1120	R	c	2016/11/20 12-36th hour
R1124	R	c	2016/11/24 12-36th hour
CT12	CT	c	2016/11/26 12-36th hour
CT24/Ec	CT	c	2016/11/26 24-48th hour
CT24/Enc	CT	nc	2016/11/26 24-48th hour

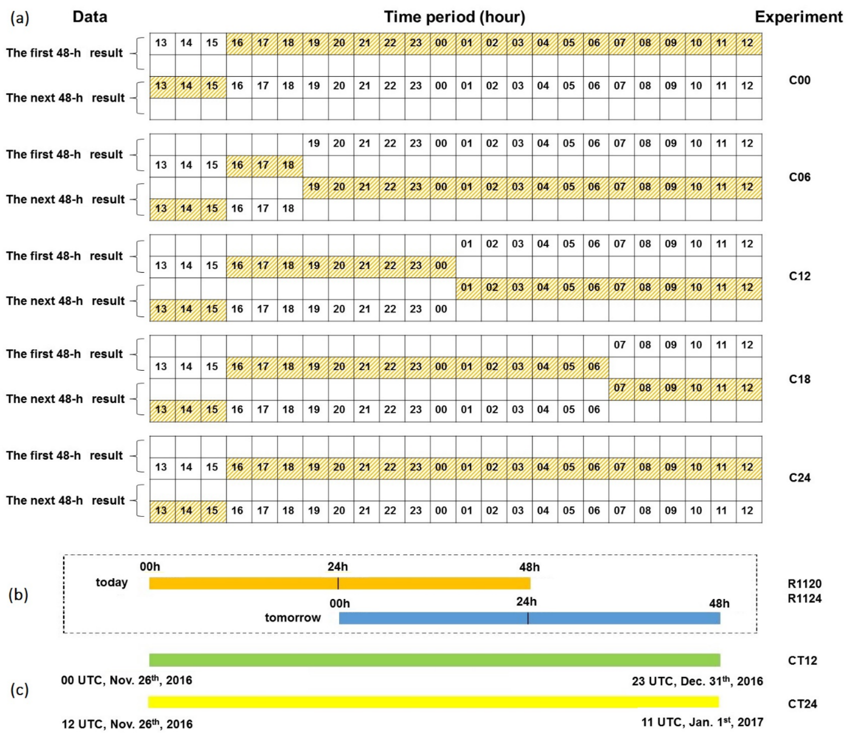

Figure 7. The time period for each initial condition experiments. **(a)** shows the time period for Clean initial condition (mark C) experiments. The first hour results in the output files of CAMx were at 13:00 UTC every day, and the CAMx model forecasted the next 48 hours' $PM_{2.5}$ concentrations in each cycle simulation. The sensitivity experiments C00, C06, C12, C18, and C24 extract different time periods (0~24h, 6~30h, 12~36h, 18~42h and 24~48h, respectively) in each output file as valid data, represented by the grids with number. Each grid represents an hour and the numbers on the grids indicate the hours of the data. The grids with numbers represents the valid time period for each output file. In order to analyze from 0:00 Beijing time (16:00 UTC) every day, the 24-hour data of a day is cut and merged from 16:00 UTC in the valid time period of each output file. And the shaded grids represent the data for one single day. **(b)** shows the time period for Restart (mark R) experiments. The meteorological data of the period 12~36 h was cut to estimate the $PM_{2.5}$ concentrations by restart simulation.

删除的内容: initialized

The first day of the simulation starts at 12:00 UTC, and the following days starts at 00:00 UTC. **(c)** show the time period for ConTinuous simulation (mark CT) experiments. The meteorological data of the period 12~36 h is cut and merged to one file for CT12 and the period 24~48 h was cut and merged for CT24.

4 Results and discussion

In this study, we collected the observations in December 2016, and evaluate the model performance and improvement. The model ability from both the meteorological field and the daily $PM_{2.5}$ simulations in Xi'an is evaluated in this study.

4.1 Model performance of the initial condition tests

There are 13 NSAQ Stations in Xi'an which marked as squares in Fig 2. Nine stations are in urban Xi'an， including GYC, XQ, FZC, XZ, TYC, GXXQ, JKQ, QJ and GYT. Three stations are located in suburban towns, including CAQ, YLQ and LTQ. The CT Station is the city background station, which is in northern urban Xi'an.

4.1.1 Sensitivity experiments for using clean initial condition files

Taylor nomogram (Taylor, 2001; Gates et al., 1999) is used to evaluate the accuracy of simulated $PM_{2.5}$ daily concentrations for NSAQ stations which was for the sensitivity experiments of using the clean initial condition files, shown in Fig 8. There are three statistical parameters to evaluate model accuracy, which are the correlation coefficient (R), normalized standard deviation (NSD), normalized root, and mean square error (NRMSE) in Taylor nomogram (Taylor, 2001; Gates et al., 1999; Chang et al., 2004). The sensitivity experiments C00, C06, C12, C18, and C24 were shown by symbols of different colors. We randomly selected 3 stations in urban Xi'an, 2 stations in county towns and a background station to show the simulation results. And the "AVG" meant the average of 13 NSAQ Stations.

As shown in Fig 8, R is 0.36-0.76 for the sensitivity experiments C00, C06, C12, C18, and C24. C24's R is largest and best over all the NSAQ Stations, and C00's is lowest. The NRMSE, which measures the distance from the marker to the REF in Taylor nomogram, is smallest and best for C24, and longest for C00. For NSD, most NSAQ Stations have similar regularity, that is, the NSD values from C00 to C24 are getting closer to "1". The other statistical parameters are presented in Table 4. From experiments C00 to C24, the absolute mean bias (MB) and the mean error (ME) decrease from 51.07 $\mu g/m^3$ to 3.72 $\mu g/m^3$ and from 74.09 $\mu g/m^3$ to 45.82 $\mu g/m^3$, respectively. The absolute normal mean bias (NMB) and the normal mean error (NME) decrease from 29.73% to 2.17% and from 43.12%to 26.67%, respectively. And the index of agreement (IOA) increase from 0.50 to 0.8. In general, the model performance of C24 is better than other sensitivity experiments in clean initial simulation tests.

删除的内容: c

删除的内容: t

删除的内容: The time period for each initial condition experiments. **(a)** shows the time period for C experiments. The output files of CAMx were initialized at 13:00 UTC every day and the CAMx model forecasted the next 48 hours' $PM_{2.5}$ concentrations. The grids with number represent the valid period of each output file. The shaded grids represent the data for one single day, which is extracted by cutting and merging the data of the valid period. **(b)** and **(c)** show the time period for R and CT experiments, respectively.

删除的内容: mechanism

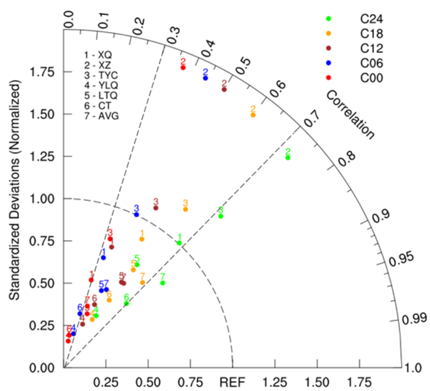

Figure 8. Taylor nomogram for modelled and observed daily averaged $PM_{2.5}$ concentrations for the sensitivity experiment of using the clean initial condition files. The "AVG" meant the average of 13 NSAQ Stations. The sensitivity experiments C00, C06, C12, C18, and C24 were shown by symbols of different colors. REF represents a perfect simulated result according to Chang et al. (2004) for air quality model.

删除的内容: The NSAQ Stations, which in urban city and county towns, have different model performances presented in Fig 8. The model performances of XZ, TYC, XQ in urban city are of poor qualities. On the contrary, YLQ and LTQ in county towns have better model performances than stations in urban city.

4.1.2 Sensitivity experiments for using restart files

In order to explore the restart simulation, sensitivity experiments R1120 and R1124 were set according to the time of the first day for the model simulation. Starting from 12:00 UTC on November 24th, the $PM_{2.5}$ concentration simulation results of the two sensitive experiments, R1120 and R1124, were shown in Fig 9. At first, the results of the two sensitivity experiments were very different, and then the two lines were gradually fitted until 16:00 UTC on November 25th. After 16:00 UTC on November 25th, the two lines fitted almost completely. Therefore, the spin-up time of 27 hours can eliminate the error brought by the initial field for the $PM_{2.5}$ concentrations in CAMx model.

删除的内容: mechanism

As shown in Table 4, the model performances of the sensitivity experiments R1120 and R1124 are similar in December, 2016. For the sensitivity experiments R1120 and R1124, the R value between observations and simulations is 0.70. The mean bias (MB) and the mean error (ME) are 4.01 μg/m^3 and 49.68 μg/m^3, respectively. The normal mean bias (NMB) and the normal mean error (NME) are 2.33% and 28.92%, respectively. The value of root mean square error (RMSE) is 67.28 and the IOA reaches 0.82.

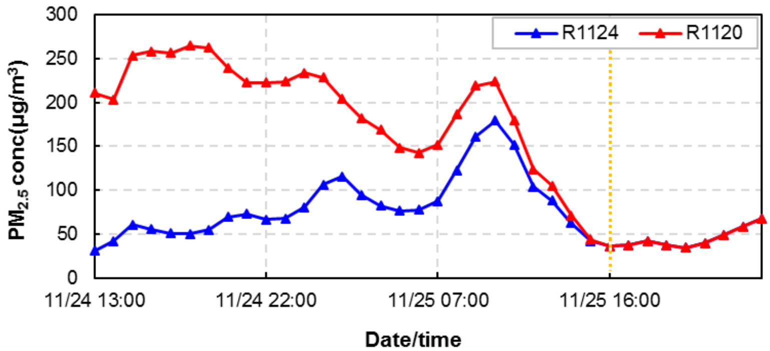

Figure 9. The time series of hourly simulated $PM_{2.5}$ concentrations for using the restart files during a period of the spin-up time. The red and blue lines represent the model sensitivity experiments R1120 and R1124, respectively. The begin day of R1120 for model simulation was November 20th, 2016, and R1124 was November 24th, 2016.

4.1.3 Sensitivity experiments for continuous simulation

As for the continuous simulation, sensitivity experiments CT12 and CT24 were conducted. Although the sensitivity experiments CT12 and R1120 use different methods to generate the initial concentration fields, the start time of the intercepted time periods for the two experiments are the same. $PM_{2.5}$ concentrations of CT12 and R1120 are presented in Fig 10. As shown in Fig 10, the points lie very close to the perfect line "y=x", which indicates that the simulation results of CT12 and R1120 were nearly identical.

The model starting time of sensitivity experiments CT12 and CT24 are November 26th 00:00UTC and November 26th 12:00UTC, respectively. The concentration accumulation of CT24 is 12 hours more than that of CT12. As shown in Fig 11 there is an air pollution peak in December 2016, which CT24 matches better than CT12. The statistical parameters of CT12 and CT24 are presented in Table 4. The mean bias (MB) and mean error (ME) of CT24 results are 6.29 μg/m^3 and 42.67 μg/m^3, respectively, a little better than the CT12 results. The root mean square error (RMSE) of CT24 results is 68.21, also slightly better than the CT12 results. From CT12 to CT24, the R and IOA increase from 0.69 to 0.81 and from 0.81 to 0.90, respectively. Thus, the sensitivity experiments CT24 has better model performance than CT12.

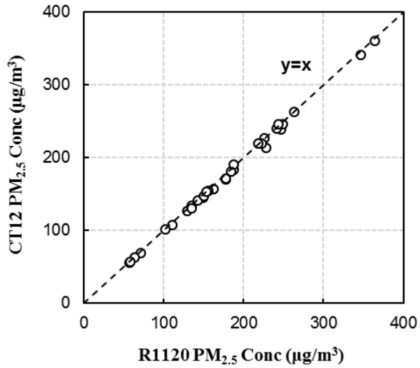

Figure 10. Scatter diagram of the R1120 and CT12 experiments of $PM_{2.5}$ concentrations. Line "y=x" represents the simulated of R1120 is the same to CT12.

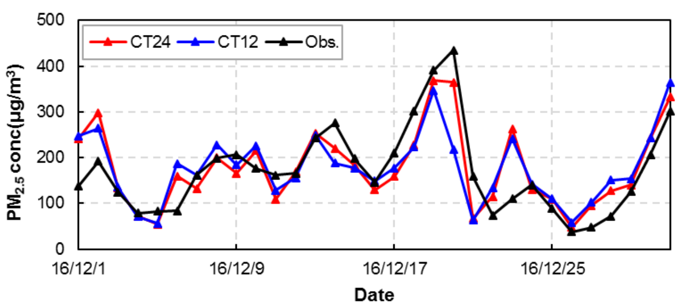

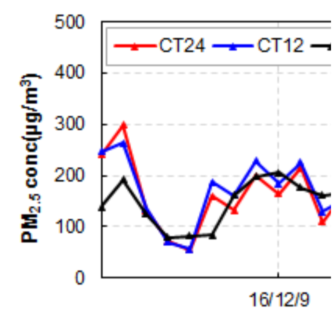

删除的内容:

Figure 11. The time series of daily $PM_{2.5}$ concentrations for continuous simulation in Xi'an. The black line represents observations, the blue and red lines show simulated data started at November 26th 00:00UTC and November 26th 12:00UTC, respectively.

4.2 Model performance of emission tests

Taylor nomogram for modelled and observed daily averaged $PM_{2.5}$ concentrations for all initial condition sensitivity experiments, shown in Fig 13. The red symbols indicate the sensitivity experiment for using the clean initial condition files, the blue symbols represent the sensitivity experiment for using the restart files, and the brown symbols show the sensitivity experiment for continuous simulation. One experiment per symbol. The circles and triangles represent “bias”. As shown in Fig 13, R is 0.36 ~ 0.81 in all initial condition sensitivity experiments. R of CT24 is the largest and best in all initial condition sensitivity experiments. The marker of CT24 has the shortest distance to the “REF” than other initial condition sensitivity experiments, which means that the NRMSE is the smallest. The NSD of CT24 is 0.92, which determines the modeled and observed patterns have more consistent amplitude of variation. According to these statistical parameters, the sensitivity experiments CT24 have the best model performance than other initial condition sensitivity experiments.

Based on the initial condition tests, we selected the best method, CT24, to do the emission sensitivity experiments, shown in Fig 12. CT24 is the experiment with construction fugitive dust emissions (sensitivity experiments Ec) and the sensitivity experiments Enc is not. As shown in fig 12, the simulated $PM_{2.5}$ concentrations of Ec play the better model performance than that of Enc in the high concentration range. As the results shows in Fig 13, R of Ec and Enc are 0.81 and 0.85, respectively. The NRMSE for Enc is smaller than Ec shown in the taylor nomogram. However, the NSD of Ec, 0.92, is better than Enc, 0.74. And the bias of Enc is much larger than Ec. The other statistical parameters are presented in Table 4. The ME decreased from 49.18 μg/m^3 to 42.67 μg/m^3 and the IOA of simulation results with the updated local emissions reached 0.90. Thus, compared to the simulation results based on the original emission inventory, a new simulation results, which were driven by the updated local emissions, showed a much better performance on $PM_{2.5}$ concentrations.

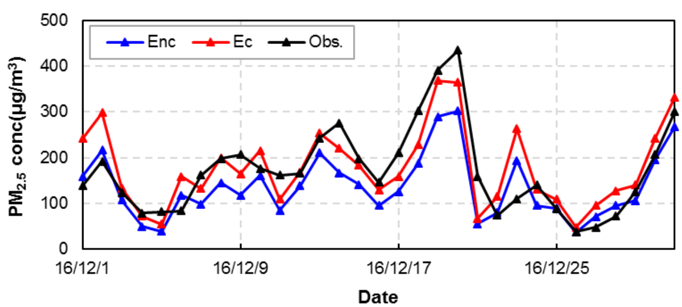

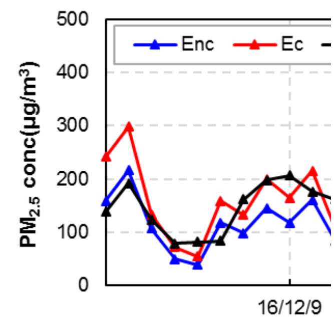

删除的内容:

Figure 12. The time series of daily observed and simulated $PM_{2.5}$ concentrations averaged from 13 NSAQ Observation Stations during December 2016 in Xi’an. The black line represents the observations, the blue line represents the simulated by the CAMx model with construction fugitive dust, and the red line represents the simulated values without construction fugitive dust.

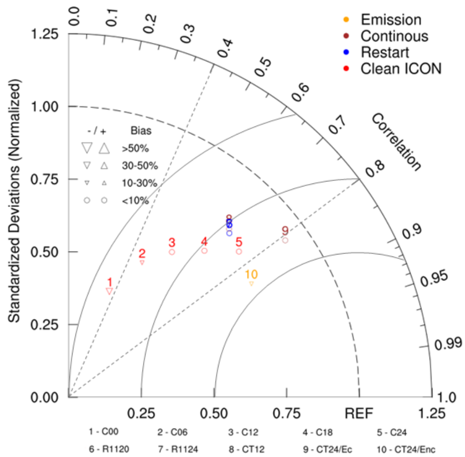

Figure 13. Taylor nomogram for modelled and observed daily PM$_{2.5}$ concentrations for all sensitivity experiments under different initial conditions and emissions. The red symbols indicate the clean initial simulation, the blue symbols represent the restart simulation, the brown symbols show the sensitivity experiment for continuous simulation, and the orange symbols are for emission tests. The triangles and circles signify "Bias". The scale of the triangle's size represents bias value and the direction of the triangle's vertex represents positive or negative.

删除的内容: mechanism

删除的内容: mechanism

Table 4. Statistical measures of the modelled daily PM$_{2.5}$ in Xi'an, unit: μg/m.3.

	R	MB(μg/m^3)	ME(μg/m^3)	NMB%	NME%	RMSE	IOA
C00	0.36	-51.07	74.09	-29.73	43.12	100.72	0.49
C06	0.48	-24.17	60.95	-14.07	35.48	85.50	0.61
C12	0.58	-12.88	53.25	-7.50	30.99	76.64	0.70
C18	0.68	-7.00	48.83	-4.08	28.42	68.85	0.78
C24	0.76	-3.72	45.82	-2.17	26.67	60.12	0.86
R1120	0.70	4.01	49.68	2.33	28.92	67.28	0.82
R1124	0.70	4.01	49.68	2.33	28.92	67.28	0.82
CT12	0.69	6.73	50.20	3.92	29.22	68.21	0.81
CT24/Ec	0.81	6.29	42.67	3.66	24.83	55.29	0.90
CT24/Enc	0.85	-35.16	49.18	-20.47	28.63	61.22	0.86

4.3 Model performance of SO_2 and NO_2

The sulfur dioxide (SO_2) and nitrogen dioxide (NO_2) concentrations are the important precursors of SO_4 and NO_3, parts of particulate matter. Daily observed and simulated SO_2 and NO_2 concentrations averaged from 13 NSAQ Stations under the initial restart simulation. Figure 2 shows the time series of daily average SO_2 and NO_2 concentrations averaged from 13 NSAQ Stations under the initial restart simulation, and the statistical results are listed in Table 1. The model has an obvious overestimation of SO_2, with an average bias of 156.31 μg/m^3, and the observed SO_2 concentration is only 18% of the simulated value. The main reason is that the implementation of desulfurization projects for important emission sources such as coal-fired power plants in recent years has not been fully considered, which has led to overestimation of SO_2 emissions in the emission inventory. Li et al. (2017b) found that the SO_2 emissions in China have decreased by 75% during the year 2007 to 2016, that is, SO_2 emissions in 2016 were about 25% of 2007. Also the intensity of emissions reduction has uneven spatial distribution. The model performance of NO_2 concentration is better, the IOA reaches 0.82, and the MB is only 3.32μg/m^3. There is high consistency of variation trend between the simulated and observed concentrations of SO_2 and NO_2, with R being 0.81 and 0.75, respectively.

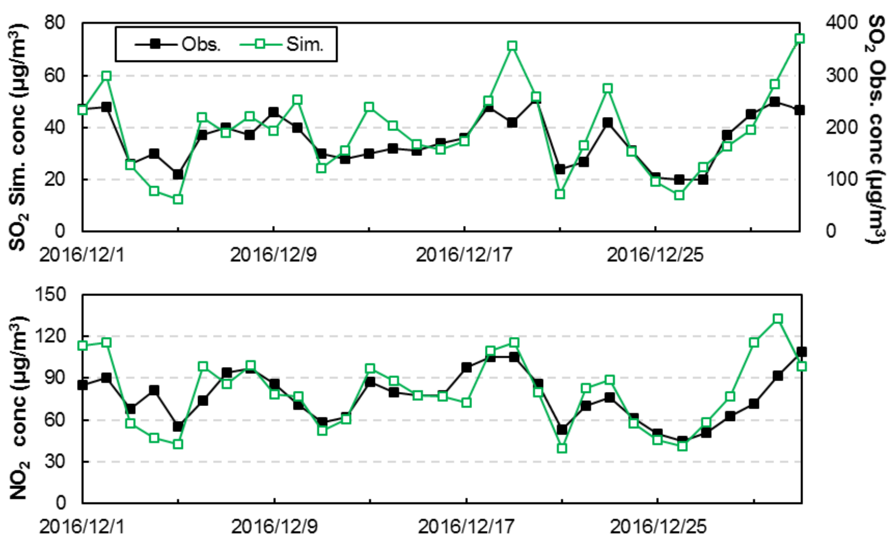

Figure 14. The time series of daily observed and simulated SO_2 (top)and NO_2 (bottom) concentrations averaged from 13 NSAQ Stations during December 2016 in Xi'an. The black and green lines indicate observed and simulated results, respectively.

带格式的: 下标

带格式的: 下标

带格式的: 正文, 缩进: 首行缩进: 1 字符

删除的内容: Observation

删除的内容: Observation

带格式的: 正文

删除的内容: Observation

Table 5. Statistical verification parameters of SO_2 and NO_2 during December 2016in Xi'an.

Species	Mean(μg/m^3)		R	MB	ME	NMB	NME	RMSE	IOA
	Obs.	Sim.		(μg/m^3)	(μg/m^3)				
SO_2	35.45	191.76	0.81	156.31	156.31	4.41	4.41	171.73	0.11
NO_2	76.77	80.09	0.75	3.32	12.86	0.04	0.17	17.13	0.82

5 Conclusions

The WRF-SMOKE-CAMx model system has been used to simulate the fine particular ($PM_{2.5}$) concentrations in Xi'an in December, 2016. In this study, the emissions of construction fugitive dust in Xi'an were added in the SMOKE to update the local emission inventory. A series of model sensitivity experiments for the initial conditions and emissions are designed to improve the model performance in the megacity, Xi'an.

Three methods were applied for the initial condition tests: using the clean initial condition files as clean initial simulation, using the restart files as restart simulation and continuous simulation. All initial condition sensitivity experiments are driven by the updated emission inventories. The emission tests are based on the initial condition sensitivity experiment which has the best model performance.

Comparing the model performance of $PM_{2.5}$ concentrations in different model sensitivity experiments in Xi'an, we found that the model combining the method of continuous simulation with the updated local emission inventory can nicely improve the model performance. According to statistical parameters, for initial condition tests, the model performance of CT24, C24 and R1120/R1124 are the best. R ranges from 0.36 to 0.81 in all initial condition sensitivity experiments. R of CT24 is the largest and best in all initial condition sensitivity experiments. R of C24 and R1120/R1124 can reach 0.76, 0.70, respectively. The MB of CT24, C24 and R1120/R1124 are lower, which are 6.29 μg/m^3, -3.72 μg/m^3 and 4.01 μg/m^3, respectively. The IOA of CT24, C24 and R1120/R1124 all reach above 0.8, of which CT24 is 0.9. Compared with other methods, the method of using the clean initial condition files has longer simulation time and larger data volume. Therefore, the method of continuous simulation for hindcast, which is to retrieve $PM_{2.5}$ concentrations is suggested. For air quality forecast, we can give priority to the method of restart simulation. Also, for simulating $PM_{2.5}$ concentrations by CAMx model, the simulate needs the spin-up time at least 27 hours. This can improve the simulation effect and reduce the simulation time.

This study updated the emissions inventory, which added construction fugitive dust emissions to the original emissions inventory. Compared to the simulation results based on the original emission inventory, a new simulation results, which were driven by the updated local emissions, showed a much better performance on $PM_{2.5}$ modelling. The absolute MB decreased from 35.16 μg/m^3 to 6.29 μg/m^3 and the IOA of simulation results with the updated local emissions reached 0.90. Therefore, the right addition of emissions will also help to improve the effects of simulation and forecasting.

带格式表格

带格式的: 正文

删除的内容: 4

删除的内容: mechanism

删除的内容: mechanism

删除的内容: mechanism

In finally, we recommend the method of continuous simulation for hindcast, which has the best model performance of $PM_{2.5}$ concentrations, and can also reduce the output of IO files to improve computing efficiency. For forecast, the method of restart simulation is suggested, which can reach similar model performance as the continuous simulation. If the restart simulation cannot be used due to the limitation of computing resources and storage space when forecasting $PM_{2.5}$ concentrations, try to extend the spin-up time as much as possible, at least 27 hours according to this work.

删除的内容: mechanism

删除的内容: mechanism

Code and data availability

The source codes of the WRF model version 3.9.1.1 used in this study are available online at https://www2.mmm.ucar.edu/wrf/users/download/get_source.html(NCAR, 2020, last access: 4 June 2020). The CAMx version 6.1 code is available at http://www.camx.com/download/default.aspx(ENVIRON, 2020, last access: 4 June 2020), and the SMOKE version 2.4 code is available at https://www.cmascenter.org/smoke/ (CMAS, 2020, last access: 4 June 2020). The global final analysis data (FNL) are from https://rda.ucar.edu/datasets/ds083.2/(NCEP, 2000, last access: 4 June 2020). The dataset related to this manuscript is available online via ZENODO (https://doi.org/10.5281/zenodo.3824676)(Xiao et al., 2020).

Author contribution

Han Xiao did the simulation and prepared the materials. Qizhong Wu designed the WRF-SMOKE-CAMx modelling system for Xi'an, including emission processes. Xiaochun Yang collected the local emission inventory in Shaanxi province and help emission processes. Lanning Wang and Huaqiong Cheng help to prepare the model dataset and figure.

Acknowledgements

The National Key R&D Program of China (2017YFC0209805), the National Natural Science Foundation of China (41305121) and the Beijing Advanced Innovation Program for Land Surface funded this work.

Appendix A

Statistical parameters for the model evaluation:

Mean bias (MB):

$$\mathrm{MB} = \frac{\sum(M_i - O_i)}{n} \quad \text{(A1)}$$

Mean error (ME):

$$\mathrm{ME} = \frac{\sum|M_i - O_i|}{n} \quad \text{(A2)}$$

Normalized mean bias (NMB):

$$\mathrm{NMB} = \frac{\sum(M_i - O_i)}{\sum O_i} \qquad \text{(A3)}$$

Normalized mean error (NME):

$$\mathrm{NME} = \frac{\sum|M_i - O_i|}{\sum O_i} \qquad \text{(A4)}$$

Root Mean Square Error (RMSE):

$$\mathrm{RMSE} = \left[\frac{1}{n}\sum_{i=1}^{n}(M_i - O_i)^2\right]^{\frac{1}{2}} \qquad \text{(A5)}$$

Correlation coefficient (R)：

$$\mathrm{R} = \frac{\sum_{i=1}^{n}(M_i - \bar{M})(O_i - \bar{O})}{\sqrt{\sum_{i=1}^{n}(M_i - \bar{M})^2 \sum_{i=1}^{N}(O_i - \bar{O})^2}} \qquad \text{(A6)}$$

Index of agreement (IOA):

$$\mathrm{IOA} = 1 - \frac{\sum_{i=1}^{n}(M_i - O_i)^2}{\sum_{i=1}^{n}(|M_i - \bar{O}| + |O_i - \bar{O}|)^2} \qquad \text{(A7)}$$

Normalized Standard Deviations (NSD):

$$\mathrm{NSD} = \frac{\sqrt{\frac{\sum_{i=1}^{n}(M_i - \bar{M})^2}{n}}}{\sqrt{\frac{\sum_{i=1}^{n}(O_i - \bar{O})^2}{n}}} \qquad \text{(A8)}$$

In the equations, M_i and O_i represent the simulated value and observation value of a station, respectively. n represents the number of stations. $\bar{M}$ and $\bar{O}$ represent the average value of simulated value and observation value, respectively.

References

Appel, K. W., Napelenok, S. L., Foley, K. M., Pye, H. O. T., Hogrefe, C., Luecken, D. J., Bash, J. O., Roselle, S. J., Pleim, J. E., Foroutan, H., Hutzell, W. T., Pouliot, G. A., Sarwar, G., Fahey, K. M., Gantt, B., Gilliam, R. C., Heath, N. K., Kang, D., Mathur, R., Schwede, D. B., Spero, T. L., Wong, D. C., and Young, J. O.: Description and evaluation of the Community Multiscale Air Quality (CMAQ) modeling system version 5.1, Geosci. Model Dev., 10, 1703–1732, https://doi.org/10.5194/gmd-10-1703-2017, 2017.

Briggs, G.: Discussions on chimney plumes in neutral and stable surroundings, Atmos. Environ., 6, 507–510, 1972.

Briggs, G.A.: Plume rise and buoyancy effects, Atmospheric Science and Power Production, 327–366, 1984.

Cao, G., Zhang, X., Gong, S., An, X., and Wang, Y.: Emission inventories of primary particles and pollutant gases for China, Chinese Sci. Bull., 56, 781–788, https://doi.org/10.1007/s11434-011-4373-7, 2011.

Cao, J.J., Shen, Z.X., Chow, J.C., Watson, J.G., Lee, S.C., Tie, X.X., Ho, K.F., Wang, G.H., and Han, Y.M.: Winter and summer $PM_{2.5}$ chemical compositions in fourteen Chinese cities, J. Air Waste Manage., 62, 1214–1226, https://doi.org/10.1080/10962247.2012.701193, 2012.CCCPSC: The Pollution Source Census Data Set (Statistic), Collected Works about the First China Pollution Source Survey Data (V), Compilation Committee of China Pollution Source Census I, China Environment Science Press, Beijing, 228–245, 2011.

CCCPSC: The Pollution Source Census Data Set (Statistic), Collected Works about the First China Pollution Source Survey Data (V), Compilation Committee of China Pollution Source Census I, China Environment Science Press, Beijing, 228–245, 2011.

Chang, J.S., Brost, R.A., Isaksen, I.S.A., Madronich, S., Middleton, P., Stockwell, W.R., and Walcek, C.J.: A three-dimensional eulerian acid deposition model: physical concepts and formulation, J. Geophys. Res.-Atmos., 92, 14681-14700, https://doi.org/10.1029/JD092iD12p14681, 1987.

Chang, J. and Hanna, S.: Air quality model performance evaluation, Meteorology and Atmospheric Physics, 87, 167-196, https://doi.org/10.1007/s00703-003-0070-7, 2004.

Chen, H. S., Wang, Z. F., Li, J., Tang, X., Ge, B. Z., Wu, X. L., Wild, O., and Carmichael, G. R.: GNAQPMS-Hg v1.0, a global nested atmospheric mercury transport model: model description, evaluation and application to trans-boundary transport of Chinese anthropogenic emissions, Geosci. Model Dev., 8, 2857–2876, https://doi.org/10.5194/gmd-8-2857-2015, 2015.

CMAS: SMOKE version 2.4, available at: https://www.cmascenter.org/smoke/, last access: 4 June 2020.

Colella, P., and Woodward, P.R.: The Piecewise Parabolic Method (PPM) for Gas-dynamical Simulations, J. Comput. Phys., 54, 174-201, https://doi.org/10.1016/0021-9991(84)90143-8, 1984.

Dobson, J.E., Bright, E.A., Coleman, P.R., Durfee, R.C., and Worley, B.A.: Landscan: a global population database for estimating populations at risk, Photogramm. Eng. Rem. S., 66, 849–857, 2000.

Dudhia, J.: Numerical study of convection observed during the winter monsoon experiment using a mesoscale two-dimensional model, J. Atmos. Sci. 46, 3077-3107, https://doi.org/10.1175/1520-0469(1989)046<3077:NSOCOD>2.0.CO;2, 1989.

Dudhia, J.: A multi-layer soil temperature model for MM5, The Sixth PSU/ NCAR Mesoscale Model Users' Workshop, Boulder, Colorado, 1996.

Eder, B., and Yu, S.: A performance evaluation of the 2004 release of Models-3 CMAQ, Atmos. Environ., 40,4811-4824, https://doi.org/10.1016/j.atmosenv.2005.08.045, 2006.

ENVIRON: User Guide for Comprehensive Air Quality Model with Extensions Version 6.0, available at: http://www.camx.com/files/camxusersguide_v6-00.pdf, 2013.

ENVIRON: CAMx version 6.1, available at: http://www.camx.com/download/default.aspx, last access: 4 June 2020.

Gates, W., Boyle, J., Covey, C., Dease, C., Doutriaux, C., Drach, R., Fiorino, M., Gleckler, P., Hnilo, J., Marlais, S., Phillips, T., Potter, G., Santer, B., Sperber, K., Taylor, K., and Williams, D.: An overview of the results of the atmospheric model inter-comparison project, B. Am. Meteorol. Soc., 80, 29–55, https://doi.org/10.1175/1520-0477(1999)080<0029:AOOTRO>2.0.CO;2, 1999.

Gilliam, R. C., Hogrefe, C., Godowitch, J. M., Napelenok, S., Mathur, R., and Rao, S. T.: Impact of inherent meteorology uncertainty on air quality model predictions, J. Geophys. Res.-Atmos., 120, 12259–12280, https://doi.org/10.1002/2015JD023674, 2015.

Grell, G.A., Peckham, S. E., Schmitz, R., Mckeen, S. A., Frost, G., Skamarock, W. C., and Eder, B.: Fully coupled "online" chemistry within the WRF model, Atmos. Environ., 39, 6957-6975, https://doi.org/10.1016/j.atmosenv.2005.04.027, 2005.

Hertel O., Berkowics, R., Christensen, J. and Hov, Ø.: Test of two numerical schemes for use in atmospheric transport-chemistry models, Atmos. Environ., 27, 2591-2611, https://doi.org/10.1016/0960-1686(93)90032-T, 1993.

Hong, S.Y., Dudhia, J., and Chen, S.H.: A revised approach to ice microphysical processes for the bulk parameterization of clouds and precipitation, Mon. Weather Rev., 132, 103-120. https://doi.org/10.1175/1520-0493(2004)132<0103:ARATIM>2.0.CO;2, 2004.

Hong, S.Y., Noh, Y., and Dudhia, J.: A new vertical diffusion package with an explicit treatment of entrainment processes, Mon. Weather Rev., 134, 2318-2341, https://doi.org/10.1175/MWR3199.1, 2006.

Houyoux, M. R. and Vukovich, J. M.: Updates to the Sparse Matrix Operator Kernel Emissions (SMOKE) modeling system and integration with Models-3, The Emission Inventory: Regional Strategies for the Future, Air Waste Management Association, Raleigh, N. C., 1461, 1999.

Huang, R. J., Zhang, Y., Bozzetti, C., Ho, K. F., Cao, J., Han, Y., Daellenbach, K., Slowik, J., Platt, S., Canonaco, F., Zotter, P., Wolf, R., Pieber, S., Bruns, E., Crippa, M., Ciarelli, G., Piazzalunga, A., Schwikowski, M., Abbaszade, G., and Prevot, A.: High secondary aerosol contribution to particulate pollution during haze events in China, Nature, 514, 218–222, https://doi.org/10.1038/nature13774, 2014.

Kain, J. S.: The Kain–Fritsch convective parameterization: An update, J. Appl. Meteorol., 43, 170–181, https://doi.org/10.1175/1520-0450(2004)043<0170:TKCPAU>2.0.CO;2, 2004.

Kato N, and Akimoto H.: Anthropogenic emission of SO_2 and NO_x in Asia: Emission inventories, Atmos. Environ., 26, 2997–3017, https://doi.org/10.1016/0960-1686(92)90291-R, 1992.

Li, L., Chen, C. H., Fu, J. S., Huang, C., Streets, D. G., Huang, H. Y., Zhang, G. F., Wang, Y. J., Jang, C. J., Wang, H. L., Chen, Y. R., and Fu, J. M.: Air quality and emissions in the Yangtze River Delta, China, Atmos. Chem. Phys., 11, 1621-1639, https://doi.org/10.5194/acp-11-1621-2011, 2011.

Li, L., Cheng, S. Y., Li, J. B., Lang, J. L., and Chen, D. S.: Application of MM5-CAMx- PSAT modeling approach for investigating emission source contribution to atmospheric SO_2 pollution in Tangshan, Northern China, Math. Probl. Eng., 2013, 1-12, https://doi.org/10.1155/2013/136453, 2013.

Li, X., Zhang, Q., Zhang, Y., Zhang, L., Wang, Y., Zhang, Q., Li, M., Zheng, Y., Geng, G., Wallington, T., Han, W., Shen, W., and He, K.: Attribution of $PM_{2.5}$ exposure in Beijing–Tianjin–Hebei region to emissions: implication to control strategies, Sci. Bull., 62, 957–964, https://doi.org/10.1016/j.scib.2017.06.005, 2017a.

Li C, Mclinden C, Fioletov V, et al.: India Is Overtaking China as the World's Largest Emitter of Anthropogenic Sulfur Dioxide, Scientific Reports, 7(1), 14304, https://doi.org/10.1038/s41598-017-14639-8, 2017b.

Li, X. B., Liu, H. B., Zhang, Z. Y., and Liu, J. J.: Numerical simulation of an extreme haze pollution event over the North China Plain based on initial and boundary condition ensembles, Atmospheric and Oceanic Science Letters, 12, 434-443, https://doi.org/10.1080/16742834.2019.1671136, 2019.

Long, X., Li, N., Tie, X., Cao, J., Zhao, S., Huang, R., Zhao, M., Li, G., and Feng, T.: Urban dust in the Guanzhong Basin of China, part I: A regional distribution of dust sources retrieved using satellite data, Sci. Total Environ., 541, https://doi.org/10.1016/j.scitotenv.2015.10.063, 1603-1613, 2016.

Mlawer, E.J., Taubman, S.J., Brown, P.D., Iacono, M.J., and Clough, S.A.: Radiative transfer for inhomogeneous atmospheres: RRTM, a validated correlated-k model for the longwave. J. Geophys. Res. Atmos. 102, 16663-16682, https://doi.org/10.1029/97JD00237, 1997.

NCAR: WRF model, available at: https://www2.mmm.ucar.edu/wrf/users/download/get_source.html, last access: 4 June 2020.

National Centers for Environmental Prediction/National Weather Service/NOAA/U.S. Department of Commerce. 2000, updated daily. NCEP FNL Operational Model Global Tropospheric Analyses, continuing from July 1999. Research Data Archive at the National Center for Atmospheric Research, Computational and Information Systems Laboratory. https://doi.org/10.5065/D6M043C6, last access: 4 June 2020.

Nenes, A., Pandis, S.N., and Pilinis, C.: Continued development and testing of a new thermodynamic aerosol module for urban and regional air quality models, Atmos. Environ., 33, 1553-1560, https://doi.org/10.1016/S1352-2310(98)00352-5, 1999.

Ni, T. R., Han, B., and Bai, Z. P.: Source Apportionment of PM_{10} in Four Cities of Northeastern China, Aerosol Air Qual. Res., 12, 571-582, https://doi.org/10.4209/aaqr.2011.12.0243, 2012.

Ohara, T., Akimoto, H., Kurokawa, J., Horii, N., Yamaji, K., Yan, X., and Hayasaka, T.: An Asian emission inventory of anthropogenic emission sources for the period 1980–2020, Atmos. Chem. Phys., 7, 4419–4444, https://doi.org/10.5194/acp-7-4419-2007, 2007.

Panagiotopoulou, A., Charalampidis, P., Fountoukis, C., Pilinis, C., and Pandis, S. N.: Comparison of PMCAMx aerosol optical depth predictions over Europe with AERONET and MODIS measurements, Geosci. Model Dev., 9, 4257–4272, https://doi.org/10.5194/gmd-9-4257-2016, 2016.

Seaman, N. L.: Meteorological modeling for air-quality assessments, Atmos. Environ., 34, 2231–2259, https://doi.org/10.1016/S1352-2310(99)00466-5, 2000.

Seinfeld, J.H., and Pandis, S.N.: Atmospheric Chemistry and Physics, From Air Pollution to Climate Change, John Wiley and Sons, Inc., New York. 1998.

Sistla, G., Zhou, N., Hao, W., Ku, J.-Y., Rao, S. T., Bornstein, R., Freedman, F., and Thunis, P.: Effects of uncertainties in meteorological inputs on Urban Airshed Model predictions and ozone control strategies, Atmos. Environ., 30, 2011–2025, https://doi.org/10.1016/1352-2310(95)00268-5, 1996.

Skamarock, W.C., Klemp, J.B., Dudhia, J., Gill, D.O., Barker, D.M., Duda, M.G., Huang, X.Y., Wang, W., and Powers, J.G.: A Description of the Advanced Research WRF Version3 (No. NCAR/TN-475+STR), University Corporation for Atmospheric Research, https://doi.org/10.5065/D68S4MVH. NCAR, 2008.

Streets, D. G., Bond, T. C., Carmichael, G. R., Fernandes, S. D., Fu, Q., He, D., Klimont, Z., Nelson, S. M., Tsai, N. Y., Wang, M. Q., WOO, J. –H., and Yarber K. F.: An inventory of gaseous and primary aerosol emissions in Asia in the year 2000, J. Geophys. Res.-Atmos., 108, 8809-8831, https://doi.org/10.1029/2002JD003093, 2003.

Tang, X., Wang, Z. F., Zhu, J., Gbaguidi, A., and Wu, Q. Z.: Ensemble-Based Surface O3 Forecast over Beijing, Climatic and Environmental Research, 15, 677–684, 2010 (in Chinese).

Taylor, K.: Summarizing multiple aspects of model performance in a single diagram, J. Geophys. Res.-Atmos., 106, 7183–7192, https://doi.org/10.1029/2000JD900719, 2001.

Wang, H., Chen, H., Wu, Q., Lin, J., Chen, X., Xie, X., Wang, R., Tang, X., and Wang, Z.: GNAQPMS v1.1: accelerating the Global Nested Air Quality Prediction Modeling System (GNAQPMS) on Intel Xeon Phi processors, Geosci. Model Dev., 10, 2891–2904, https://doi.org/10.5194/gmd-10-2891-2017, 2017.

Wang, L. T., Zhang, Q., Hao, J. M., and He, K. B.: Anthropogenic CO emission inventory of Mainland China, Acta Scientiae Circumstantiae, 25, 1580–1585, https://doi.org/10.13671/j.hjkxxb.2005.12.002, 2005 (in Chinese).

Wang, P., Cao, J. J., Shen, Z., Han, Y., Lee, S. C., Huang, Y., Zhu, C. S., Wang, Q., Xu, H., Huang, R. J.: Spatial and seasonal variations of PM2.5 mass and species during 2010 in Xi'an, China, Sci. Total Environ., 508, 477-487. https://doi.org/10.1016/j.scitotenv.2014.11.007, 2015.

Wang, Z., Xie, F., Wang, X., An, J., and Zhu, J.: Development and application of nested air quality prediction modeling system, Chinese Journal of Atmospheric Science, 30, 778–790, https://doi.org/10.3878/j.issn.1006-9895.2006.05.07, 2006 (in Chinese).

Wu, D., Fung, J. C. H., Yao, T., and Lau, A. K. H.: A study of control policy in the Pearl River Delta region by using the particulate matter source apportionment method, Atmos. Environ., 76, 147-161, https://doi.org/10.1016/j.atmosenv.2012.11.069, 2013.

Wu, Q., Wang, Z., Gbaguidi, A., Tang, X., and Zhou, W.: Numerical study of the effect of traffic restriction on air quality in Beijing, Sola, 6 (Special Edition), 17–20, https://doi.org/10.2151/sola.6A-005, 2010.

Wu, Q. Z., Xu, W. S., Shi, A. J., Li, Y. T., Zhao, X. J., Wang, Z. F., Li, J. X., and Wang, L. N.: Air quality forecast of PM_{10} in Beijing with community multi-scale air quality modeling (CMAQ) system: emission and improvement, Geosci. Model Dev., 7, 2243–2259, https://doi.org/10.5194/gmd-7-2243-2014, 2014.

Xiao, H., Wu, Q., Yang, X., Wang, L., Cheng, H.: The dataset of the manuscript "Numerical study of the initial condition and emission on simulating PM2.5 concentrations in Comprehensive Air Quality Model with extensions version 6.1 (CAMx v6.1): Taking Xi'an as example", Zenodo, https://doi.org/10.5281/zenodo.3824676, 2020.

Xiao, H., Yang, X. C., Wu, Q. Z., Bai, Q. M., Cheng, H. Q., Chen, X. S., Xue, R., Du, M. M., Huang, L., Wang, R. R., and Wang, H.: Estimate emissions of construction fugitive dust in Xi'an, Acta Scientiae Circumstantiae, 39, 222-228, https://doi.org/10.13671/j.hjkxxb.2018.0377, 2019 (in Chinese).

Yang, X., Wu, Q., Zhao, R., Cheng, H., He, H., Ma, Q., Wang, L., and Luo, H.: New method for evaluating winter air quality: $PM_{2.5}$ assessment using Community Multi-Scale Air Quality Modeling (CMAQ) in Xi'an, Atmos. Environ., 211, 18-28, https://doi.org/10.1016/j.atmosenv.2019.04.019, 2019.

Yang, X., Xiao, H., Wu, Q., Wang, L., Guo, Q., Cheng, H., Wang, R., and Tang, Z.: Numerical study of air pollution over a typical basin topography: Source appointment of fine particulate matter during one severe haze in the megacity Xi'an, Sci. Total Environ., 708, 135213, https://doi.org/10.1016/j.scitotenv.2019.135213, 2020.

Yarwood. G., Rao, S., Yocke, M., and Whitten, G. Z.: Updates to the Carbon Bond chemical mechanism: CB05, Final Report prepared for US EPA. available at: http://www.camx.com/publ/pdfs/CB05_Final_Report_120805.pdf, 2005.

Zhang, L., Brook, J. R., and Vet, R.: A revised parameterization for gaseous dry deposition in air-quality models. Atmos. Chem. Phys., 3, 2067–2082, https://dx.doi.org/10.5194/acp-3-2067-2003, 2003.

Zhang, L., Gong, S., Padro, J., Barrie, L.: A size-segregated particle dry deposition scheme for an atmospheric aerosol module, Atmos. Environ., 35, 549-560, https://doi.org/10.1016/S1352-2310(00)00326-5, 2001.

Zhang, Q., Streets, D. G., Carmichael, G. R., He, K., Huo, H., Kannari, A., Klimont, Z., Park, I., Reddy, S., Fu, J. S., Chen, D., Duan, L., Lei, Y., Wang, L., and Yao, Z.: Asian emissions in 2006 for the NASA INTEX-B mission, Atmos. Chem. and Phys., 9, 5131–5153, https://doi.org/10.5194/acp-9-5131-2009, 2009.

Zhang, Q., Klimont, Z., Streets, D. Huo, H. and He, H.: An anthropogenic PM emission model for China and emission inventory for the year 2001, Progress in Natural Science, 16, 223–231, 2006 (in Chinese).

Zhang, X.Y., Cao, J.J., Li, L.M., Arimoto, R., Cheng, Y., Huebert, B., and Wang, D.: Characterization of atmospheric aerosol over Xi'an in the south margin of the Loess Plateau, China, Atmos. Environ., 36, 4189–4199, https://doi.org/10.1016/S1352-2310(02)00347-3, 2002.

Zhang, Y., Bocquet, M., Mallet, V., Seigneur, C., and Baklanov, A.: Real- Time Air Quality Forecasting, Part I: History, techniques, and current status, Atmos. Environ., 60, 632-655, https://doi.org/10.1016/j.atmosenv.2012.06.031, 2012.

Zhang, Y. P., Li, X., Nie, T., Qi, J., Chen, J., and Wu, Q.: Source apportionment of $PM_{2.5}$, pollution in the central six districts of Beijing, China, J. Clean. Prod., 174, 661-669, https://doi.org/10.1016/j.jclepro.2017.10.332, 2018.

Supplement

Table S1 shows the statistical results of the daily average $PM_{2.5}$ concentrations of 13 NSAQ Observation Stations during December 2016 in Xi'an. The correlation coefficients (R) of most urban stations can reach above 0.6, of which GYC is 0.73, while the R of XQ, QJ and XZ are low. Among the three stations in suburban counties, CAQ had the highest correlation coefficient of 0.68, and the other two stations are lower than 0.6. For bias, the model performances of stations in urban cities are better than that of the suburbs, and the simulated $PM_{2.5}$ concentrations in the suburbs are obviously underestimated. Except for CT, GYT and XZ, the FAC2 of the other 7 urban stations all reach more than 70%. Among the three suburban stations the CAQ has the best model performance, with FAC2 at 86%, while the other two stations are relatively low, especially the YLQ is only 31%. The average FAC2 of the urban cities is 74%, while the average FAC2 of the suburban counties is 62%, indicating that the model performance of the urban area is better than that of the suburban area in terms of total emissions.

Table S1. Verification statistics of PM2.5 concentrations on December 2016 among all monitoring sites.

	Station	R	MB ($\mu g/m^3$)	ME ($\mu g/m^3$)	NMB %	NME %	RMSE	FAC2 %
	CT	0.70	-58.86	66.22	-38.08	42.84	89.99	64
	XQ	0.53	61.72	81.41	36.00	47.48	108.31	75
	JKQ	0.69	-76.00	84.91	-37.55	41.95	109.89	76
	TYC	0.66	75.46	89.90	45.98	54.78	108.49	77
urban	GYC	0.73	19.42	52.51	11.17	30.21	68.01	89
	QJ	0.59	14.79	71.73	8.06	39.11	89.90	76
	GYT	0.62	-31.46	69.01	-18.72	41.06	84.15	66
	FZC	0.67	3.11	60.68	1.79	35.01	76.42	78
	XZ	0.57	51.62	79.66	32.64	50.36	101.86	72
	GX	0.64	67.11	88.46	39.42	51.96	104.45	69
	CAQ	0.68	8.51	54.49	5.36	34.29	72.26	86
suburban	YLQ	0.60	-97.63	99.12	-57.67	58.55	120.78	31
	LTQ	0.57	-54.43	76.28	-33.53	46.98	97.49	69

Appendix SA

Statistical parameters for the model evaluation:

Fraction of predictions within a factor of two of observations(FAC2):

$$0.5 \le \frac{M_i}{O_i} \le 2.0 \qquad \text{(SA1)}$$